Journal of Human Evolution 191 (2024) 103517

Contents lists available at ScienceDirect

Journal of Human Evolution

journal homepage: www.elsevier.com/locate/jhevol

Virtual reconstruction and geometric morphometric analysis of the Kocabaş hominin fossil from Turkey: Implications for taxonomy and evolutionary significance

Tommaso Mori [a, b, *], Alessandro Riga [b], Ahmet Ihsan Aytek [c], Katerina Harvati [a, d]

[a] Paleoanthropology, Institute for Archaeological Sciences and Senckenberg Centre for Human Evolution and Palaeoenvironment, Eberhard Karls University of Tübingen, Rümelinstraasse 23, 72072, Tübingen, Germany
[b] Anthropology Laboratory, Department of Biology, University of Florence, Via del Proconsolo 12, 50122, Florence, Italy
[c] Department of Anthropology, Burdur Mehmet Akif Ersoy University, Faculty of Arts and Science, TR-15030, Burdur, Turkey
[d] DFG Centre for Advanced Studies "Words, Bones, Genes, Tools", Eberhard Karls University of Tübingen, Rümelinstraasse 23, 72072, Tübingen, Germany

ARTICLE INFO

Article history:
Received 12 December 2022
Accepted 26 February 2024
Available online 22 May 2024

Keywords:
Eastern Mediterranean
Early Pleistocene
Middle Pleistocene
Virtual anthropology
Ballik travertine

ABSTRACT

The Kocabaş specimen comes from a travertine quarry near the homonymous village in the Denizli basin (Turkey). The specimen comprises three main fragments: portions of the right and left parietal and left and right parts of the frontal bone. The fossil was assumed to belong to the *Homo erectus* s.l. hypodigm by some authors, whereas others see similarities with Middle Pleistocene fossils (Broken Hill 1/Kabwe, Bodo, or Ceprano). Here, we present the first attempt to make a complete reconstruction of the missing medial portion of the frontal bone and a comprehensive geometric morphometric analysis of this bone. We restored the calotte by aligning and mirroring the three preserved fragments. Afterward, we restored the missing portion by applying the thin-plate spline interpolation algorithm of target fossils onto the reconstructed Kocabaş specimen. For the geometric morphometric analyses, we collected 80 landmarks on the frontal bone (11 osteometric points, 14 bilateral curve semilandmarks, and 41 surface semi-landmarks). The comparative sample includes 21 fossils from different chronological periods and geographical areas and 30 adult modern humans from different populations. Shape analyses highlighted the presence in Kocabaş of features usually related to Middle Pleistocene *Homo*, such as a developed supraorbital torus associated with a relatively short frontal squama and reduced post-toral sulcus. Cluster analysis and linear discriminant analysis classification procedure suggest Kocabaş being part of the same taxonomic unit of Eurasian and African Middle Pleistocene *Homo*. In light of our results, we consider that attributing the Kocabaş hominin to *H. erectus* s.l. may be unwarranted. Results of our analyses are compatible with different evolutionary scenarios, but a more precise chronological framework is needed for a thorough discussion of the evolutionary significance of this specimen. Future work should clarify its geological age, given uncertainties regarding its stratigraphic provenance.

1. Introduction

Human dispersal and the human route 'out of Africa' played a major role in the early phases of human evolution. The earliest human remains outside the African continent currently known are dated to 1.77 Ma at the site of Dmanisi, Georgia (Gabunia and Vekua, 1995). However, Early and early Middle Pleistocene *Homo* fossils from Eurasia are scarce, resulting in a gap between this early dispersal and the more recent and relatively abundant Middle Pleistocene human fossil record. The fossil hominin from Kocabaş from the Denizli Basin in Turkey, recovered in 2002 from a travertine quarry near the Kocabaş village (Kappelman et al., 2008), can help shed light on early human presence in Eurasia.

Workers discovered the Kocabaş remains during the processing of the travertine blocks brought from the travertine area to the factory (Dalmersan), as reported by Mehmet Cihat Alçiçek (Kappelman et al., 2008). There, the blocks were sliced at ca. 35 cm of thickness. The partial calotte was embedded in one of the blocks and, unfortunately, was cut by the saw used in the factory. The process only left three fragments of the skullcap: a large fragment

* Corresponding author.
E-mail address: tommaso.mori@unifi.it (T. Mori).

https://doi.org/10.1016/j.jhevol.2024.103517

of the right parietal, a fragment of the right frontal preserving part of the supraorbital torus, and a partial left parietal articulated with a fragment of the left frontal bone (not preserving the supraorbital torus). The exact provenance of the hominin find is not known (Kappelman et al., 2008). Nevertheless, it is considered that it likely derives from the Upper Travertine level, which was the only one exploited at the time of discovery in 2002 (Vialet et al., 2012; Lebatard et al., 2014). This level also yielded various Pleistocene faunal remains, such as *Equus, Dama, Stephanorhinus* sp., *Bison* sp., *Bos,* and *Testudo* sp. (Boulbes et al., 2014; Lebatard et al., 2014). Based on the thermoluminescence dating of the sediments at the specimen's presumed location, a first geological age of 510 ± 50 to 330 ± 30 ka was suggested for the travertines (Kappelman et al., 2008). However, since thermoluminescence has an upper limit of ca. 500 ka, a Turkish–French team carried on a paleomagnetic study of a sequence of travertine sediments (Vialet et al., 2012). The authors proposed an older age of more than 780 ka for the fossil-bearing sediments. A more detailed paleomagnetic and cosmogenic analysis of the sequence of travertine sediments conducted by Lebatard et al. (2014) showed that the levels exhibited reverse polarity. The authors, therefore, suggested that they were deposited before the Cobb Mountain subchron (between ca. 1.50 and 1.22 Ma). Lebatard et al. (2014) concluded that the Kocabaş specimen has a chronological age most likely between 1.1 and 1.3 Ma. This older chronology was supported by Khatib et al. (2014), who in their stratigraphic, sedimentological, and paleomagnetic study of the region also proposed an age between 1.5 and 1.2 Ma for the Upper Travertine of Kocabaş. Lastly, a U/Th analysis of the travertine suggest a precipitation age with a minimum age comprised between 0.55–1.31 Ma (Claes et al., 2020). The Kocabaş skullcap, therefore, potentially fills a paleoanthropological gap between 1.5 and 1.0 Ma, observed in both the African and the Eurasian fossil records. Indeed, this record is scarce in the time period between ca. 1.6–1.5 Ma (i.e., Kenya's fossils such as KNM-ER 3773) and ca. 1 Ma (*Homo erectus*-like hominins from East Africa: KNM-OG 45500, BOU-VP-2/66 Daka, UA 31). In Africa, among the few specimens falling in this period are the recently recovered DAN5/P1 and BSN12/P1 specimens from Gona, Ethiopia, dated to around 1.6–1.5 and 1.26 Ma (Semaw et al., 2020; Baab et al., 2022), OH 9 may be as old as 1.47 Ma (Schwartz and Tattersall, 2005), but given the uncertainty about its exact provenance, it could be younger; craniodental remains from Konso (Suwa et al., 2007) were also dated around 1.4 Ma. In Europe, there are few known specimens from this time period: apart from the deciduous tooth from the Orce Basin dated to ca. 1.4 Ma (Toro-Moyano et al., 2013), the oldest human fossils are the Atapuerca–Sima del Elefante highly fragmentary remains, dated to ca. 1.2 Ma (Carbonell et al., 2008). East Asia's oldest known paleoanthropological evidence was recovered from the Sangiran dome and was dated to around 1.3 Ma (Matsu'ura et al., 2020). The geographical provenance and proposed early chronology of the Kocabaş individual, therefore, make this specimen pivotal for our understanding of the transition and relationship between Early Pleistocene *Homo erectus* s.l. and later Middle Pleistocene human populations.

A preliminary description and comparative analysis of the Kocabaş cranium were conducted by Kappelman et al. (2008). These authors provisionally attributed it to *H. erectus* s.l. on the basis of nonmetric features and a few linear measurements. Important traits included the prominent supraorbital torus, which Kappelman et al. (2008) found to resemble Javanese and African *H. erectus* s.l., rather than Chinese representatives of the species; and a distinct post-toral sulcus, commonly considered as a typical *H. erectus* condition (Kappelman et al., 2008). This first conclusion was supported by several subsequent studies (Guipert et al., 2011; Vialet et al., 2012, 2014, 2018). Linear measurement analysis and cladistic analysis supported the conclusion that Kocabaş belonged to *H. erectus* s.l. hypodigm (Vialet et al., 2012, 2018). However, works based on a geometric morphometric (GM) approach did not convincingly support such a taxonomic affiliation. Only two GM comparative shape analyses have been published to date (Vialet et al., 2014; Aytek and Harvati, 2016), both showing that the Kocabaş frontal morphology is similar both to *H. erectus* s.l. and to Middle Pleistocene African (Broken Hill 1/Kabwe and Bodo; Vialet et al., 2014) or Eurasian fossils (Ceprano and Arago; Aytek and Harvati, 2016). In their work, Vialet et al. (2014) proposed a morphological similarity between OH 9 and Kocabaş. It is important to notice that already in this analysis, Vialet et al. (2014) found similar shapes between Bodo, Broken Hill 1/Kabwe, and Kocabaş (plotting very close in their principal component analysis). However, in their discussion, they concluded that Kocabaş belonged to *H. erectus* s.l. without discussing the close vicinity in shape space between Kocabaş and Middle Pleistocene fossils. Probably the grouping used, where Middle Pleistocene specimens such as Bodo and Broken Hill 1/Kabwe were assigned by Vialet et al. (2014) to African *H. erectus,* influenced the discussion and conclusion of their work. Therefore, even though their analysis showed similarities between Kocabaş and these Middle Pleistocene African specimens, this result was not discussed, and Vialet et al. (2014), instead, proposed strong morphological affinities to early *H. erectus* from Africa.

The GM analysis performed by Vialet et al. (2014) was questioned on several points by Aytek and Harvati (2016). Some of the issues pointed out were that Vialet et al. (2014) did not include a measure of supraorbital torus thickness, thus removing a critical feature in the characterization of frontal shape from their GM analysis. Therefore, the analysis performed by Aytek and Harvati (2016) focused on the supraorbital torus shape, in order to include this important feature, as well as fragmentary specimens such as OH 9. Their results showed no clear affinity of Kocabaş to OH 9. Instead, they found similarities to the later Chinese *H. erectus* s.l. and Middle Pleistocene samples. In 2018, Vialet et al. (2018) performed both a metric and a cladistic analysis, concluding again that Kocabaş belonged to *H. erectus* s.l. In the metric analysis, they included Middle Pleistocene fossils, and they grouped Broken Hill 1/Kabwe with the Middle Pleistocene European hominin fossils (Ceprano, Petralona). However, this most recent analysis also shows some shortcomings: the metric analysis performed only comprised four linear measurements. After the data collection, no size correction was performed, and the four measurements were analyzed through principal component analysis (PCA). However, especially because the sample included a wide size range (their analysis comprised small specimens such as KNM-ER 1813 as well as bigger ones such as the *Homo neanderthalensis* from La Ferrassie), these results reflected mainly size differences along the first component. This was an expected result, given the lack of size correction and the nature of PCA, an exploratory method looking for the greater source of variation. No other clear pattern or separation was found between the different samples included in the PCA. Their cladistic analysis showed a closer relation of Kocabaş to the late Early Pleistocene fossils (ca. 1 Ma) from UA 31, BOU-VP-2/66 Daka and KNM-OG 45500. However, this analysis did not include any Middle Pleistocene fossils. Therefore, it was not possible to test any relationship between Kocabaş and later hominin taxa. In conclusion, the taxonomic status of this important specimen and the affinities with Middle Pleistocene *Homo* pointed out in previous studies remain unresolved.

Here, we use virtual anthropology and semilandmark-based GM surface analysis to reconstruct and investigate the morphology of the Kocabaş frontal bone in a comparative framework, which includes *H. erectus* s.l. from Africa and Asia, as well as Middle Pleistocene *Homo* from both Eurasia and Africa. In this framework, we

also present a new reconstruction of the skullcap with a complete restoration of the frontal squama using state-of-the-art techniques in virtual anthropology (Weber, 2015).

2. Materials and methods

2.1. Frontal bone virtual reconstruction

Reconstruction of the frontal bone was conducted digitally using Avizo software v. 9.1 (Thermo Fisher Scientific, Waltham). The original fossil was scanned using a NextEngine three-dimensional (3D) surface scanner (Camera resolution: 3 Mp and accuracy: 125 μm) by A.I.A. in the Hierapolis Museum, Pamukkale, Denizli (Turkey), where the specimen is permanently stored. Afterward, the 3D meshes of the fragments were used for the virtual reconstruction. The reconstruction followed three main steps: 1) alignment of originally preserved morphology, 2) reconstruction and alignment of bilateral structures based on mirroring of existing morphology, and 3) reconstruction of missing structures by interpolation from reference specimens.

Step 1 First, the two fragments of the right parietal and left parietofrontal element were articulated following the sagittal suture and aligned using the cut plane as a reference plane to get the original curvature. After this step, to align the frontal fragment, we mirrored the previously articulated elements along the sagittal plane (Gunz et al., 2009). The mirrored specimen preserved the articulation between parietal and frontal bone at the level of stephanion along the coronal suture; this was used only as a guide to align better the original right frontal fragment to the right parietal bone. Once the right frontal fragment was aligned, the previously mirrored left frontal fragment was discarded, and the three original fragments were merged to form a complete 3D model (Fig. 1).

In order to test the reconstruction accuracy, we performed a second alignment of the original fragments at a later time.

Step 2 The two 3D meshes composed of the three fragments (left frontoparietal fragment, right frontal fragment, and right parietal fragment) derived from the two alignment processes were mirrored to reconstruct the left portion of the orbital missing part. The mirrored version of the 3D mesh was aligned using two different approaches. The first was conducted manually in a virtual environment—resulting in Kocabaş 1—following homologous anatomical structures. The second in a semiautomatic way using thin-plate spline algorithm (TPS; Bookstein, 1997; Gunz et al., 2009; Benazzi and Senck, 2011; Weber, 2015)—resulting in Kocabaş 2.

The TPS-based alignment involved registering five landmarks (bregma, stephanion left and right, and frontotemporale left and right) on both the original and the mirrored versions of the specimen and 80 semilandmarks digitized on the preserved portion of the skullcap of the original reconstructed specimen. The patch of 80 semilandmarks was projected onto the mirrored specimen and was slid using the minimum-bending-energy criterion to ensure landmark correspondence across specimens (Gunz et al., 2005). Subsequently, the mirrored specimen was warped onto the original using TPS interpolation (Bookstein, 1997) based on the landmarks and semilandmarks configuration. By warping the mirrored specimen, we deformed it to the original mesh, thereby maintaining asymmetries of the original fragments.

This approach to reconstructing the missing side was found by Benazzi and Senck (2011) to have better accuracy than a simple mirroring and aligning method and to closely match the original morphology of the missing part. After these steps, we had two slightly different 3D models (Fig. 2). To avoid confusion, in all subsequent analyses, we referred in the plot to Kocabaş 1 and Kocabaş 2 which, in turn, referred to the two different alignments made from the original fragments. Therefore, starting from these alignments, Kocabaş 1 was mirrored using a manual alignment, and Kocabaş 2 used the TPS methodology described earlier.

Step 3 In order to fully reconstruct the frontal squama and the medial aspect of the supraorbital torus, we used TPS interpolation of target fossils onto the reconstructed Kocabaş specimen (Table 1). We used six different fossils for each of the two alignments. On both reconstructions (Kocabaş 1 and Kocabaş 2), we could collect eight landmarks (landmarks number 1, 2, 4, 6, 8, 9, 10, and 11 from Table 2), 14 equally distant curves semilandmark for each temporal line, and we placed 250 surface semilandmark as a template on the preserved aspect of Kocabaş skullcap. The template was projected on all the target fossils used for the reconstruction. After projection, semilandmarks were allowed to slide using the minimum-bending-energy criterion (Gunz et al., 2005). Subsequently, we warped each fossil to the landmarks and semilandmarks configuration of Kocabaş. In conclusion, we had two different alignments Kocabaş 1 and Kocabaş 2; on each one of these alignments, we warped six different fossils (see Table 1 for a list); resulting in twelve different reconstructions of the frontal squama and the medial portion of the supraorbital torus (for an example, see Fig. 3; to see all the reconstructions, see Supplementary Online Material [SOM] Figs. S1 and S2). The twelve reconstructions, as well as the mean of the two sets of reconstructions based on different alignments, were used as individual specimens in our shape analyses (e.g., Harvati et al., 2010; Mori et al., 2020). The reconstructions after alignment of the fragments and mirroring, as well as one full reconstruction after TPS warping can be downloaded from Zenodo at the link: https://zenodo.org/records/10017514 (November 2023).

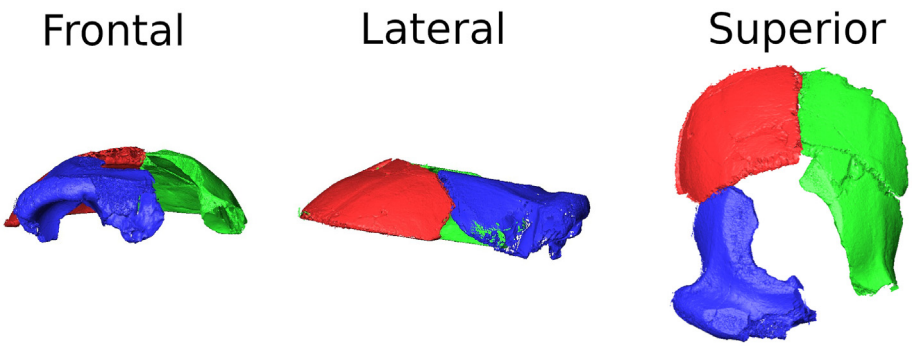

Figure 1. Alignment of the fragments in frontal, lateral, and superior view. In red, the partial right parietal bone; green, the articulated fragment of the partial left portion of the frontal bone and left parietal bone; blue, the right portion of the frontal bone.

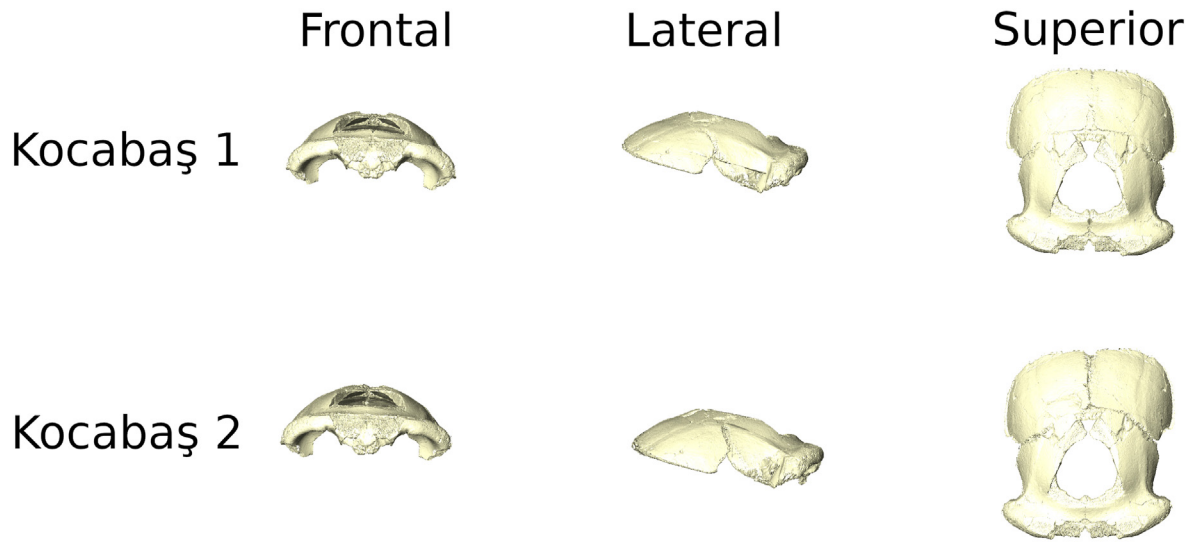

Figure 2. Kocabaş 1 made using manual alignment of mirrored better preserved bilateral structures and Kocabaş 2 made using the thin plate spline method in frontal, lateral and superior view.

Table 1
Fossil specimens used in this study.

Fossil specimen	Frontal reconstruction	Cast/ original	Institution	Chronology
Kocabaş		O	Hierapolis Museum	1.2–0.5 Ma (Vialet et al., 2012; Lebatard et al., 2014)
Homo erectus s.l.				
D 2280		C	AMNH	1.77 Ma (Garcia et al., 2010)
D 2700[a]		C	AMNH	1.77 Ma (Garcia et al., 2010)
D 3444	X	C	AMNH	1.77 Ma (Garcia et al., 2010)
D 2282[a]		C	AMNH	1.77 Ma (Garcia et al., 2010)
KNM-OG 45500[b]		O	National Museums of Kenya	900 ka (Potts et al., 2004)
BOU-VP-2/66 (Daka)	X	O	National Museum of Ethiopia	1.00–0.78 ka (Asfaw et al., 2002)
KNM-ER 3733		O	Kenya National Museum	1.63 Ma (Lepre and Kent, 2015)
KNM-ER 3883	X	O	Kenya National Museum	1.53 Ma (McDougall et al., 2012)
Ngandong 14[c]		C	AMNH	60–70 ka/130 ka, 118–108 ka (Storm et al., 2005; Yokoyama et al., 2008; Rizal et al., 2020)
Sangiran 17	X	C	AMNH	1.8–1.6/1.2 Ma/900 ka (Swisher et al. 1994; Larick et al., 2001; Matsu'ura et al., 2020)
Sambungmacan 3	X	C	AMNH	60–70 ka (Yokoyama et al., 2008)
Zhoukoudian I[d]		C	AMNH	700–400 ka (Shen et al., 2009)
Zhoukoudian 12		C	AMNH	700–400 ka (Shen et al., 2009b)
Middle-Pleistocene *Homo* (MPH)				
Ceprano		C	AMNH	430–385 ka (Manzi et al., 2010; Nomade et al., 2011; Di Vincenzo et al., 2017)
Arago		O	University of Vienna	438 ± 31 ka (Falguères et al., 2015)
Bodo		O	National Museum of Ethiopia	640–550 ka (Rightmire, 1996)
Broken Hill 1 (Kabwe)		C	AMNH	700–200 ka (Buck and Stringer, 2015; Grün et al., 2020)
Petralona	X	O	Aristotle University of Thessaloniki	700–150 ka (Grün, 1996)
Dali		C	AMNH	270–180 ka (Xiao et al., 2002)
Early *H. sapiens* (EHS)				
Jebel Irhoud 1		C	AMNH	300–90 ka (Grün and Stringer, 1991; Richter et al., 2017)
Skhūl V		O	Peabody Museum, Harvard University	120–80 ka (Grün, 2006)

Abbreviations: D, Dmanisi; KNM, Kenya National Museums; ER, East Rudolf; OG, Olorgesailie; AMNH, American Museum of Natural History.
[a] Sub-adult specimens.
[b] Also published as KNM-OL 45500. KNM-OG 45500 follows the accession number at the National Museums of Kenya.
[c] Following Schwartz and Tattersall's (2005) nomenclature.
[d] Also published as Skull I locus E (Black, 1931; Schwartz and Tattersall, 2005).

2.2. Reference sample

Our comparative sample comprises 30 recent adult modern humans from different populations of various geographical backgrounds. The sampling strategy was designed to capture high variation in recent human populations, with worldwide coverage and the inclusion of both sexes. The comparative samples are derived from museum collections and are no older than a few hundred years (see Table 3 for specific geographic origin, sex, accession number, and housing institution information). Three-dimensional surface models of the specimens were obtained from medical computed tomography (CT) scans or μCT scans using the

Table 2
Landmark number and definition.

Landmarks	Definition (Baab, 2016)	Preserved configuration	OH 9 Configuration
1. Bregma	Posterior border of the frontal bone along the midsagittal plane	X	
2. Midline post-toral sulcus	Minima of concavity on midline post-toral frontal squama	X	X
3. Glabella	Anterior-most point on frontal bone in Frankfort horizontal in the midsagittal plane		X
4/6 Mid-torus inferior R/L	Inferior margin of superior margin of orbit roughly at the middle of the orbital margin	X	X
5/7 Mid-orbital superior R/L	Superior point on the supraorbital torus at the middle of the orbital margin		X
8/9 Frontotemporale R/L	Where the temporal line reaches its most anteromedial position on the frontal	X	X
10/11 Stephanion R/L	Where the temporal line reaches the coronal suture.	X	X (only L)

Abbreviations: R, right; L, left.

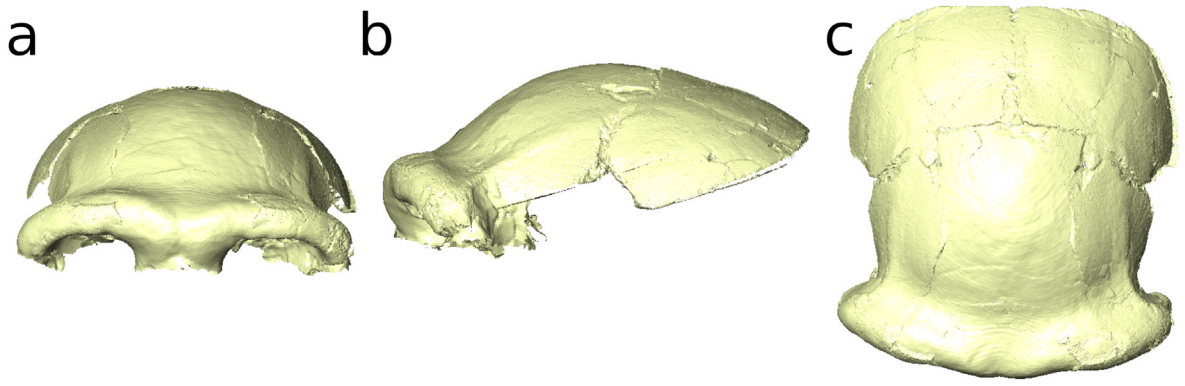

Figure 3. Full reconstruction of the medial portion of the frontal bone. Reconstruction based on the Petralona specimen. A) Frontal view; B) lateral view; C) superior view (to see all different reconstructions see SOM Figs. S1 and S2).

Table 3
Modern human samples used in this study.

Population	*n* (M/F/U)	Collections	Accession number
Australia	6 (3/3/0)	American Museum of Natural History, New York	99-8155, 99-8158, 99-8165, 99-8175, 99-8180, VL-246
Europe (Italy)	5 (2/3/0)	Museo di Storia Naturale, Florence	131, 165, 405, 412, 874
Chile (Tierra del Fuego)	3 (0/2/1)	Naturhistorisches Museum, Vienna	6031-G2, 6034-G3, 21462
Sri Lanka	4 (0/0/4)	University of Tübingen	1016, 1020, 1021, 1023
China	5 (0/0/5)	Musée de l'Homme, Paris	17570, 17571, 17572, 17574, 17575
Philippines	5 (0/0/5)	Musée de l'Homme, Paris	9758, 9759, 9763, 9764, 9868
Tanzania	2 (0/0/2)	University of Tübingen	3, 10

Abbreviations: M, male; F, female; U, unknown.

Avizo software. Information on the scans can be found in these studies (Noback and Harvati, 2014, 2015; Bosman et al., 2019, 2020; Mori et al., 2020).

The comparative fossil sample comprises 21 specimens from different chronological periods and geographical areas. The 3D surface models are derived from CT scans of the original specimens or optical surface scans of high-resolution casts (Table 1). We included several *H. erectus* s.l. fossils spanning the Pleistocene, as well as other Middle to Late Pleistocene *Homo* and to early *Homo sapiens* (Jebel Irhoud 1, Skhūl V).

2.3. Landmark digitization

We collected a total of 80 landmarks on the frontal bone. Of these, 11 correspond to common osteometric points (i.e., type 1–3 landmarks sensu Weber and Bookstein, 2011). A list and definition of the landmarks used are presented in Table 2. Two semilandmark curves (i.e., type 4 landmarks, sensu Weber and Bookstein, 2011) along each superior temporal muscle line were digitized from stephanion to the frontozygomatic suture. A total of fourteen evenly spaced semilandmarks were placed on each curve. To fully investigate the shape of the frontal squama and the supraorbital torus, we used a patch of 41 surface semilandmarks (i.e., type 6 landmarks, sensu Weber and Bookstein, 2011) encompassing the space between the previously identified landmarks (i.e., between the superior temporal muscle line and the supraorbital region). The patch was first digitized on KNM-OG 45500 and later projected on each specimen and comprised 18 symmetrical semilandmarks and five sagittal semilandmarks. Patch projection was conducted using the 'placepatch' function of the 'Morpho' v. 2.8 package (Schlager, 2017) in R v. 4.1.0 (R Core Team, 2021). The position of all landmarks is presented in Figure 4.

All landmarks were digitized by the same user (T.M.). To estimate the measurement error of fixed landmark acquisition, we digitized the same specimen 10 times in 10 different days for the 11 Type 1–3 landmark configuration. Subsequently, intraobserver error was evaluated for each landmark based on a relative standard-deviation threshold of 5%. Error assessment for these landmarks is important as they are used to delimit the placement of semilandmarks. For all 11 landmarks, the error was between 2.0% and 3.5% relative standard deviation, and thus all landmarks were used for subsequent analysis.

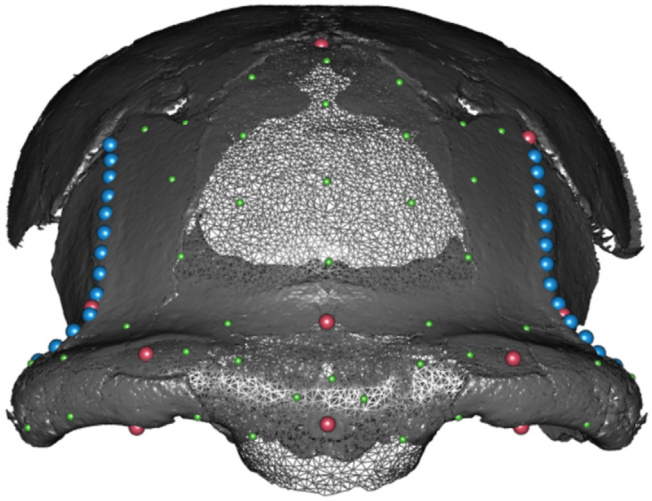

Figure 4. Landmark (red dots) and semilandmark configuration (curve semilandmarks indicated by blue dots and surface semilandmarks shown as green dots) shown on the reconstructed Olorgesailie hominin KNM-OG 45500. Image adapted from scan courtesy of the National Museums of Kenya.

2.4. Shape and statistical analysis

To explore variation in frontal bone shape in our sample, we conducted four analyses with different sample distributions and landmark sets. The first analysis used the full sample, which comprised all fossils and modern humans, and the full landmarks and semilandmarks datasets. The second analysis was conducted on a reduced landmark dataset comprising only the landmarks preserved on the original specimen, which therefore did not have to be estimated. This dataset included eight landmarks and the two temporal curves semilandmarks and was termed 'preserved configuration' dataset. The third analysis included only the landmarks/curves preserved on specimen OH 9, which made it possible to include this important individual in our comparative sample. This dataset comprised nine landmarks and only the left temporal curve and was termed the 'OH 9 configuration' dataset. The fourth analysis used the full landmarks and semilandmarks dataset but was limited to the fossil sample only.

In the first, third, and fourth analyses, we used multiple reconstructions of Kocabaş derived from multiple estimations of the frontal bone morphology based on TPS warping of reference specimens. In this case, we named Kocabaş 1 and Kocabaş 2 the mean landmarks/semilandmarks configuration of the six different reconstructions (based on different reference specimens) made for the two different mirroring alignments, where Kocabaş 1 refers to the manual alignment and Kocabaş 2 to the TPS based alignment.

In each case, we used the following procedure: a patch of surface semilandmarks (when present) was projected on each specimen. The patch was first digitized on KNM-OG 45500, and we ensured that it would be perfectly symmetrical using the 'symmetrize' function from the package 'Morpho.' Bilateral landmarks of the patch were reflected and relabeled; then both configurations were averaged to obtain a perfectly symmetric one. Curve semilandmarks and the projected surface semilandmarks (when present) were slid using the minimum-bending-energy criterion to guarantee landmark homology across specimens (Gunz et al., 2005) using 'slider3d' function in the 'Morpho' package. Thereafter, landmark configurations were superimposed using generalized Procrustes analysis (GPA; removing all Kocabaş reconstructions; Gower, 1975; Rohlf and Slice, 1990; Bookstein, 1991), in which the sum of squared distances between corresponding landmarks is minimized by rotation, translation, and scaling. After GPA superimposition, PCA (Wold et al., 1987) of the Procrustes coordinates was used to visualize and explore each shape space. In every PCA, we used the covariance matrix built on the comparative sample. Subsequently, we performed an ordinary Procrustes analysis to register the shapes of the different virtual reconstructions of Kocabaş on the mean shape of the comparative sample. Lastly, the registered landmark configurations of Kocabaş reconstructions were projected to predict its principal component (PC) score values. In this way, neither the PCA axes nor the Procrustes coordinates of our reference sample were influenced by Kocabaş itself, therefore, treating it as an unknown. We also performed two different GPA and PCA using the mean configuration of Kocabaş reconstructions as part of the sample without projecting Kocabaş specimen in the shape space. More details and results of these two analyses can be found in SOM S1. While PCA was performed without a priori group categorization, group variation along major PC axes of variation was visualized a posteriori by applying convex hulls (Mitteroecker and Bookstein, 2011). Shape variation along PCs was visualized as a deformation of a 3D surface mesh derived from the mean GPA landmark configuration or directly as a modification of landmarks' position. Vertices of the 3D surface mesh are the landmarks and semilandmarks used in the analysis. The mean surface and landmarks configuration was transformed via TPS interpolation (Bookstein, 1989) along two standard deviations of a given PC axis. In addition, in the last analysis, the shape of Kocabaş mean PC1 and PC2 scores and the mean shapes of *H. erectus* s.l. and Middle Pleistocene *Homo* were converted into triangular meshes. We display the differences between Kocabaş mesh and the comparative groups as local variation (contraction and expansion) by converting the area of each facet into a color map using the function 'localmeshdiff' embedded in the 'Arothron' v. 2.0.5 package (Profico et al., 2018, 2021, 2023). In this way, we evaluate directly the differences and similarities in surface area between Kocabaş and these two groups.

Centroid size (CS), calculated as the square root of the summed squared distances of the landmark coordinates from their centroid, is an indicator of size differences between individuals in a sample (Rohlf and Slice, 1990; Bookstein, 1991; Slice, 2007; Mitteroecker and Gunz, 2009). Usually, the first component in shape analysis shows some correlation with size; therefore, in the first analysis, we used log-transformed CS (logCS) to perform a Spearman correlation test (logCS was not normally distributed therefore we opted for a non-parametric test) between PC1 score distribution and logCS to evaluate whether the PC had an allometric component. All analyses were conducted using 'Arothron' and 'Morpho' packages (Schlager, 2017; Profico et al., 2021) in R programming language (R Core Team, 2021).

2.5. Unweighted pair group method using arithmetic averages cluster analysis

Procrustes distance, calculated as the square root of the sum of squared differences between two superimposed landmark configurations, was used as a quantitative measure for assessing overall shape affinities between specimens, with low values indicating greater shape similarity. Following the fourth analysis, the pairwise Procrustes distance matrix between all the fossils was used to perform a cluster analysis, with the unweighted pair group method using arithmetic averages (UPGMA; Sokal, 1958). We calculated the Procrustes distances for the Kocabaş reconstructions taking the mean configuration of all the different reconstructions made. This approach iteratively quantifies the similarity between two fossils and generates clusters of all sampled specimens in a rooted tree dendrogram, where all branch tips are of equal distance to the root.

Analyses were performed using the R package 'Phangorn' v. 2.8.1 (Schliep, 2011). Procrustes distances were visualized as density plots at an intraspecific and interspecific level in *H. erectus* s.l. and Middle Pleistocene *Homo*. Kocabaş's pairwise distances with all the *H. erectus* s.l. and Middle Pleistocene *Homo* specimens were plotted in the density plot to visually identify shape similarities with the comparative sample.

2.6. Linear discriminant analysis

Linear discriminant analysis (LDA) and classification analyses based on PC scores from the fourth analysis were used to classify group affiliation of all Kocabaş reconstructions. We decided to perform LDA based on PC scores from the fourth analysis because this PCA was conducted only on fossil specimens. Using PCs from previous analyses would have led the discriminant function to perform well in separating modern humans from other groups, but it would not have had good discriminant power in separating fossils. We used solely specimens belonging to two groups: *H. erectus* s.l. and the generally defined Middle Pleistocene *Homo* because the inclusion of early *H. sapiens* would have reduced the number of variables to only one in the analysis since LDA needs fewer variables than cases in each group (Lachenbruch and Goldstein, 1979). Specimens used to calculate the function, therefore, were only fossils grouped as Middle Pleistocene *Homo* and *H. erectus* s.l. We used the first four PCs as variables for the LDA, accounting for 84.04% of the total variance, and all reconstructions were treated as unknown. The number of variables for LDA needs to be lower than the number of individuals in each group. In our case, we could use maximum of five variables (5 PCs). PC5 did not meet the assumption of normal distribution; therefore, we excluded it and kept the first four PCs. The first four PCs almost (see below) met LDA assumption (Field, 2013): normal distribution, absence of outlier, similarity in covariance matrix, and homogeneity of distribution. We used histograms and Shapiro–Wilks test to verify that all PC scores showed an approximately normal distribution. Outlier detection through boxplots was performed (Field, 2013). Although Sambungmacan 3 was found to be an outlier in the PC1 scores for the *H. erectus* s.l. group and Dali an outlier in PC2 scores for the Middle Pleistocene *Homo*, we decided to keep them, given the limited number of fossils available, a common problem in paleontology. Finally, the covariance matrices were similar among groups in all components, and Box's M-tests showed that they were homogeneous for the samples ($p = 0.153$). We calculate the posterior probability of classification with SPSS software v. 24 (IBM, Armonk) for Windows. Given the small number of individuals and also the grouping affiliation that could represent a source of error in the LDA, results need to be approached with caution.

3. Results

3.1. Shape analyses

Figure 5 shows a plot of the first two components resulting from a PCA of the Procrustes coordinates including all the comparative samples and the complete landmark set, accounting for >80% of the total variance (see SOM Fig. S3 for a PCA plot without projected specimens). Together, they show a clear separation between the recent modern humans and the fossil specimens, mostly along a dimension oblique to PC1 and PC2. The second component, instead, helps to differentiate the Middle Pleistocene *Homo* fossils from *H. erectus* s.l. The distribution of PC1 values in the sample seems to reflect a temporal trend. We did not find an allometric relationship between PC1 and logCS, as the correlation test result was not statistically significant (S-score = 1240, $p = 0.3957$, rho = 0.19). Specimens such as KNM-ER 3733 or D2280 exhibit the lowest PC1 scores, with Sambungmacan 3 showing the highest PC1 scores among fossil samples (a more detailed discussion on this specimen and this morphospace can be found in Mori et al. (2020) which used a similar dataset), similar to those of the early *H. sapiens* specimens, Jebel Irhoud 1, and Skhul 5. Shape variation associated with positive PC1 scores is linked to a more rounded frontal squama with a relatively more domed frontal vault, characterizing *H. sapiens*. At negative PC1 scores, the frontal morphology exhibits a 'shelf-like' condition, with a projected glabellar region and a clear supraorbital torus with an evident post-toral sulcus and lateral constriction, features typical of the *H. erectus* s.l. frontal bone morphology. Furthermore, temporal lines are less laterally displaced and relatively longer along negative PC1 scores than in positive PC1 values, whereas positive PC1 exhibits more lateroinferiorly placed and more arched temporal lines. The supraorbital region laterally shows a flexion inferior to the frontozygomatic area for positive PC1, reflecting the reduced lateral segments of the superciliary arches in modern humans. PC2 scores are linked to the supraorbital morphology and the relative size of the frontal squama. Positive scores of PC2 are related to a more robust, thicker, and laterally wider supraorbital torus with a relatively bigger supraorbital region than the frontal squama and a less constricted frontal, morphology characteristic of Middle Pleistocene *Homo*. Negative values of PC2 show a more posteriorly elongated temporal line and proportionally more elongated frontal squama than the supraorbital region. All reconstructions of Kocabaş, including those based on *H. erectus* reference specimens, fall outside the *H. erectus* s.l. convex hull. Some reconstructions in this analysis are intermediate between Middle Pleistocene *Homo* and *H. erectus* s.l., and others are closer to the Middle Pleistocene *Homo* convex hull and closest to the African specimens Broken Hill 1/Kabwe and Bodo, although they tend to have lower PC1 values than Middle Pleistocene *Homo,* indicating a somewhat more receding forehead than most members of this group.

In a second analysis, we used only the landmarks and curve semilandmarks that were obtained directly on the Kocabaş fossil after the mirroring steps of the fragments (see Fig. 2). Therefore, only two reconstructions were used, both comprising only the existing bone fragments after manual and TPS mirroring alignment (Kocabaş 1/Kocabaş 2). Results of the PCA are presented in Figure 6. Here, PC1 and PC2 account for ca. 79% of the total variance. This reduced dataset still separates fossils and modern humans along with the first two components. However, the separation between fossil samples is less evident along PC2 than in the previous analysis: the convex hulls of Middle Pleistocene *Homo* and *H. erectus* s.l. overlap somewhat, with Broken Hill 1/Kabwe and Dali falling within the latter sample's variation. Nevertheless, specimens from the Middle Pleistocene *Homo* group still show the highest PC2 scores among all individuals. In this shape space, a positive PC1 score is linked to a relatively higher vault with temporal lines that are lower and more curved projecting lateroposteriorly. The orbital landmarks (landmark N. 4 and 6) are almost on the same coronal plane as the mid-toral sulcus and the anterior part of the temporal line in the top view. Low PC1 values are linked to a flatter frontal vault, a straight temporal line with more anteriorly projecting orbital landmarks. The mid-toral sulcus and the anterior portion of the temporal line are not on the same plane as the orbital landmarks for negative PC1 scores. Low PC2 is linked to a relatively longer frontal squama than positive PC2. The temporal lines, for positive PC2, are more laterally placed with a greater distance between temporal lines and the orbital region. Negative values of PC2 are related to a narrower postorbital constriction. As in analysis 1, Kocabaş is closer to the Middle Pleistocene *Homo* convex hull than to the *H. erectus* s.l., falling closest to African specimens such as

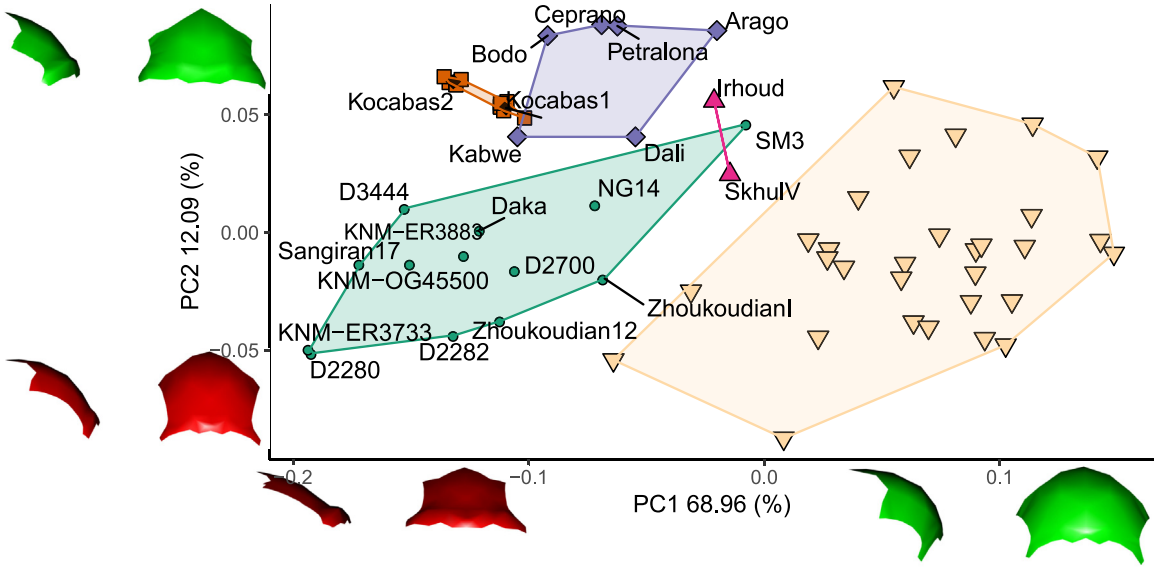

Figure 5. Plot of principal component (PC) scores 1 and 2 of the shape analysis of the full landmark configuration, including fossil specimens and recent modern humans. Convex hulls based on group attribution from Table 2. Surface shape transformations ±2 SD from mean PC values along each axis are shown below the plot for PC1 and on the left side for PC2. Symbols: yellow triangle = modern humans; green circle = *Homo erectus* s.l.; purple diamond = Middle Pleistocene *Homo*; pink triangle = early *Homo sapiens;* brown square = Kocabaş reconstructions (black diamond = mean configuration of each reconstruction).

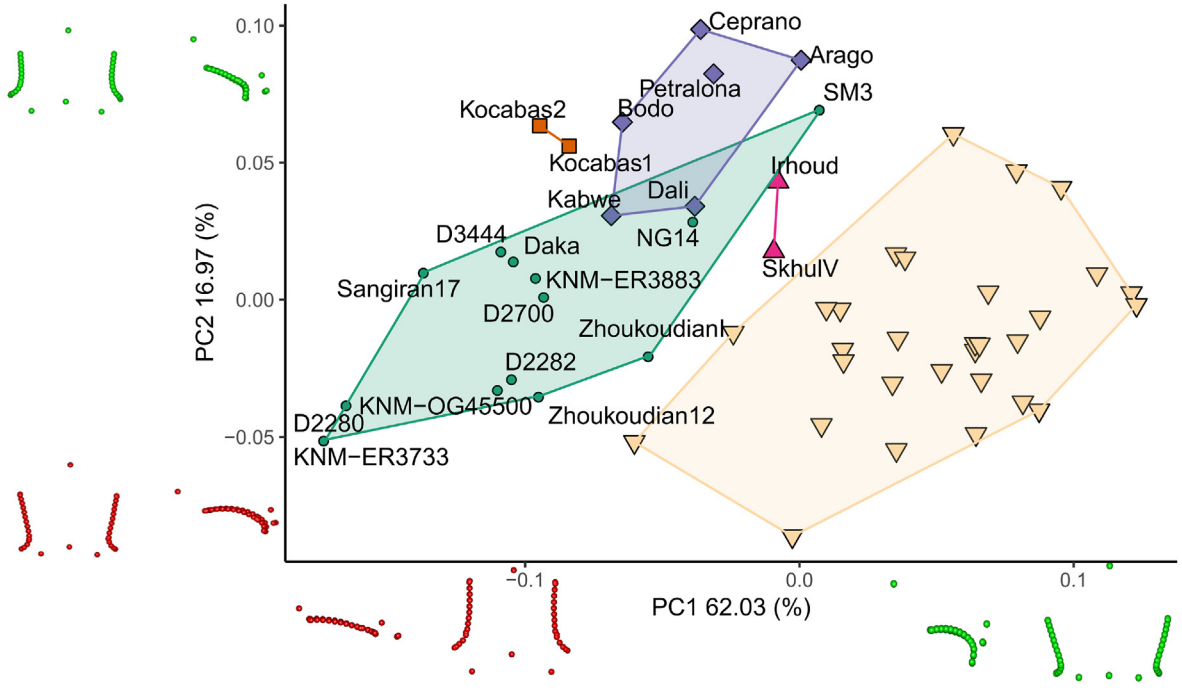

Figure 6. Plot of principal component (PC) scores 1 and 2 of the shape analysis of the 'preserved configuration', including fossil specimens and recent modern humans. Frontal landmarks (in lateral and upper views) shape variation corresponding to ±2 SD from mean PC values along each axis are shown below the plot for PC1 and to the left side for PC2. Symbols: yellow triangle = modern humans; green circle = *Homo erectus* s.l.; purple diamond = Middle Pleistocene *Homo*; pink triangle = early *Homo sapiens;* brown square = Kocabaş reconstructions (black diamond = mean configuration of each reconstruction).

Bodo and Broken Hill 1/Kabwe. However, its PC1 score is more negative than that of the former sample, indicating, again, a somewhat flatter and longer frontal in Kocabaş than in the Middle Pleistocene *Homo* specimens included here.

We conducted a third analysis based only on the limited number of landmarks/curve semilandmarks preserved on OH 9 in order to include this important specimen. Results are presented in Figure 7. PC1 and PC2 together account for ca. 70% of the total variance. This limited dataset still separates fossil and modern humans along PC1, similar to the previous two analyses. However, as in the second analysis, the convex hulls of Middle Pleistocene *Homo* and *H. erectus* s.l. overlap, with Broken Hill 1/Kabwe, Bodo, and Dali falling within the range of *H. erectus* s.l. variation. Shape changes associated with PC1 for positive scores are a vertically positioned

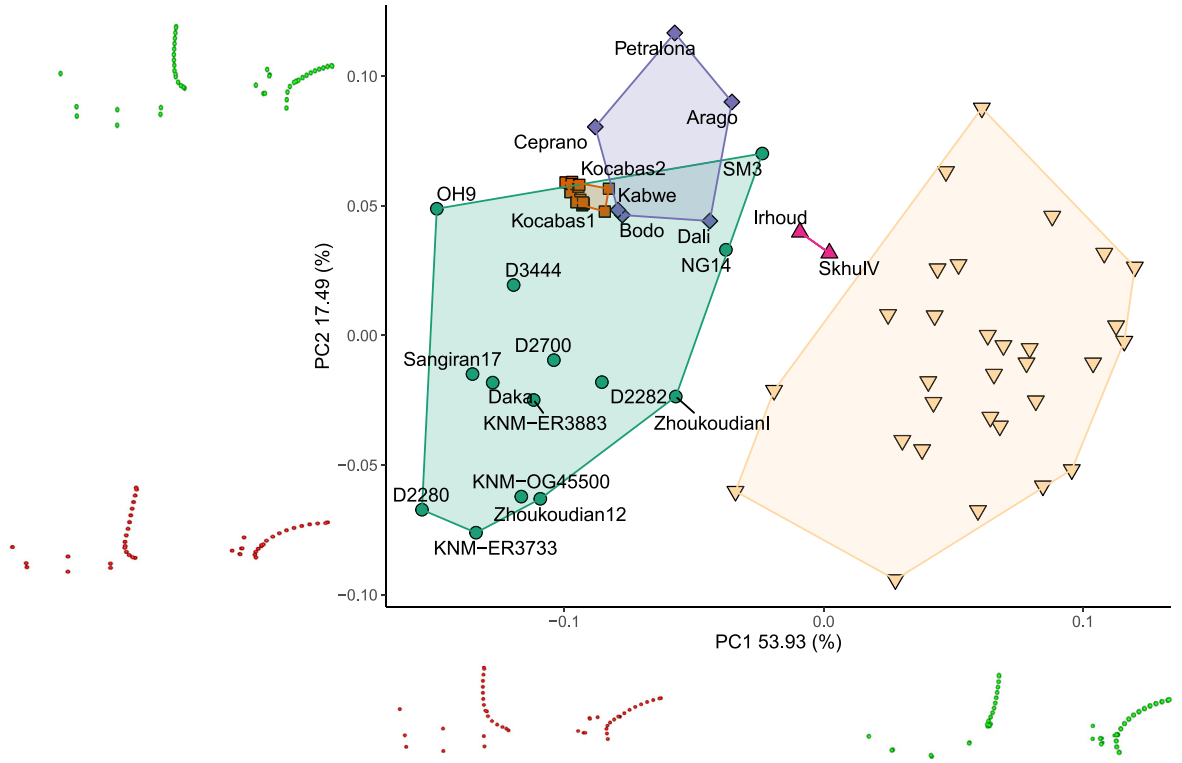

Figure 7. Plot of principal component (PC) scores 1 and 2 of the shape analysis of the 'OH 9 configuration', including fossil specimens and recent modern humans. Frontal landmarks (in lateral and upper views) shape variation corresponding to ±2 SD from mean PC values along each axis is shown below the plot for PC1 and to the left side for PC2. Symbols: yellow triangle = modern humans; green circle = *Homo erectus* s.l.; purple diamond = Middle Pleistocene *Homo*; pink triangle = early *Homo sapiens;* brown square = Kocabaş reconstructions (black diamond = mean configuration of each reconstruction).

mid-toral sulcus relative to glabella, indicating less anterior projection of the supraorbital region, a reduced thickness of the supraciliary region, and a rounder and more arched temporal line. Negative values are related to a more anteriorly projecting orbital and supraorbital landmarks (landmarks N. 4, 5, 6, 7) than the temporal line and a flatter morphology (i.e., the difference in height between stephanion and glabella). In PC2, the temporal line is shorter and more distant to the orbital region for positive scores than the negative values, indicating a more expanded trigon area of the supraorbital torus. Positive PC2 shape changes are associated with a thicker supraorbital torus with a more anteriorly placed mid toral sulcus than negative PC2. Here, again, Kocabaş is closer in its plot position to the Middle Pleistocene *Homo,* especially to the Broken Hill 1/Kabwe, and Bodo specimens from Africa. Interestingly, OH 9 does not cluster with other African Early Pleistocene *H. erectus* s.l.. Although it also plots away from Kocabaş and the other Middle Pleistocene *Homo* on PC1, it shows a similar PC2 score to Kocabaş and to the latter sample generally.

In our last shape analysis, we included only the fossil specimens but used all the landmark and semilandmarks also used in the first analysis (Fig. 8; see SOM Fig. S4 for a PCA plot without projected specimens). This PCA mirrors the first analysis in that the Middle Pleistocene *Homo* sample is well separated from that of the *H. erectus* s.l. The early *H. sapiens* specimen Skhul 5 plots close to Sambungmacan 3. Shape variation associated with positive values of the first component includes a more rounded frontal squama, post-toral sulcus reduction with wider postorbital constriction, and a relatively shortened anteroposteriorly frontal squama. Negative PC1 scores are associated with a more anteriorly projecting glabellar region; in addition, the temporal lines are less curved and more medially displaced, and the frontal squama in between them shows a flatter morphology. Postorbital constriction, as well as a marked post-toral sulcus, is evident for negative PC1 scores. The supraorbital torus also projects more laterally for negative PC1 scores. Along PC2, Middle Pleistocene *Homo* fossils tend to have higher values, whereas early *H. sapiens* have lower PC2 scores. *H. erectus* s.l. show both high and low values, with Early Pleistocene specimens toward the positive end and Middle–Late Pleistocene fossils toward the negative end. Positive scores of PC2 are associated with a thicker morphology of the supraorbital torus and an overall more robust structure. Positive PC2 is also associated with a reduction of the post-toral sulcus with the frontal squama that ends in the supraorbital torus with an almost uninterrupted shape. The frontal squama is reduced in size relative to the supraciliary region. Negative PC2 scores are associated with a weaker supraorbital torus than the relative size of the frontal squama. As in all other analyses, all reconstructions of the frontal bone of Kocabaş plot close to the Middle Pleistocene *Homo* group. They all show a relatively rounded frontal profile with a thick supraorbital torus. One of the reconstructions, the Kocabaş 2 alignment, has among the highest PC2 scores in the plot. As before, Kocabaş is closer to the Middle Pleistocene Bodo and Broken Hill 1/Kabwe specimens. Local shape differences between the Kocabaş mean PC1 and PC2 shape and average *H. Erectus* s.l. and Middle Pleistocene *Homo* shapes are reported in Figure 9. Kocabaş, compared to *H. erectus* s.l., exhibits higher values of local expansion and constriction in the frontal shape. Kocabaş is more expanded in the supraorbital torus morphology, but it is more constricted in the posterior part of the frontal squama. Differences between Kocabaş and the Middle Pleistocene *Homo* average configuration are less extreme and are related to relative constriction of the bregmatic area and local constriction of the trigon area on the supraorbital torus, medial differences in the supraorbital torus seems to suggest a

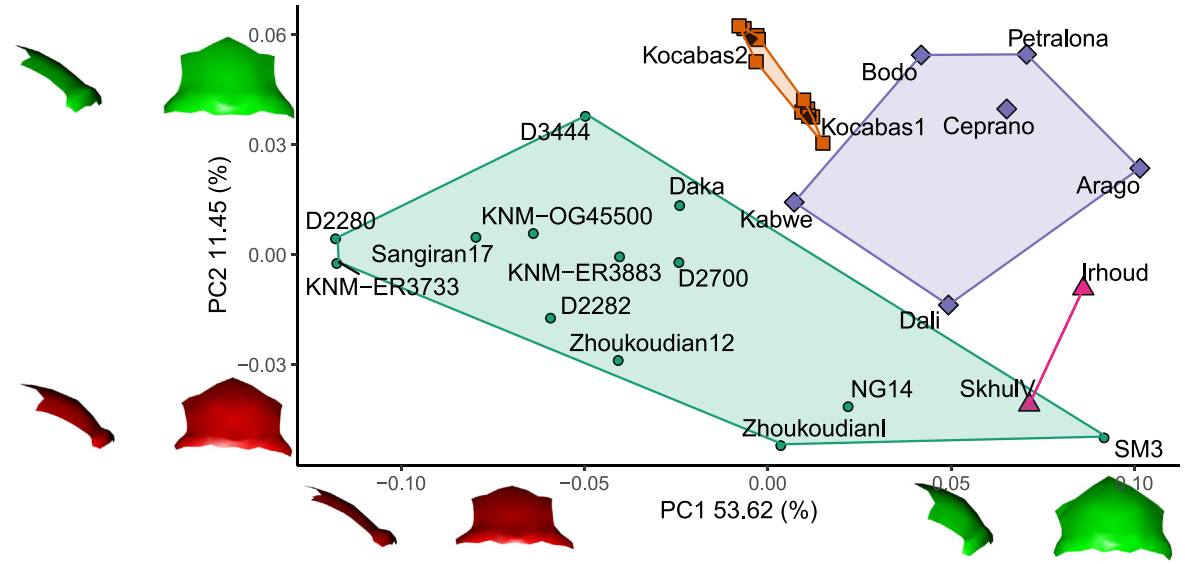

Figure 8. Plot of principal component (PC) scores 1 and 2 of the shape analysis of the full landmark configuration, including only the fossil samples. Frontal bone (in lateral and frontal views) shape variation corresponding to ±2 SD from mean PC values along each axis is shown below the plot for PC1 and to the left side for PC2. Symbols: green circle = *Homo erectus* s.l.; purple diamond = Middle Pleistocene *Homo*; pink triangle = early *Homo sapiens;* brown square = Kocabaş reconstructions (black diamond = mean configuration of each reconstruction).

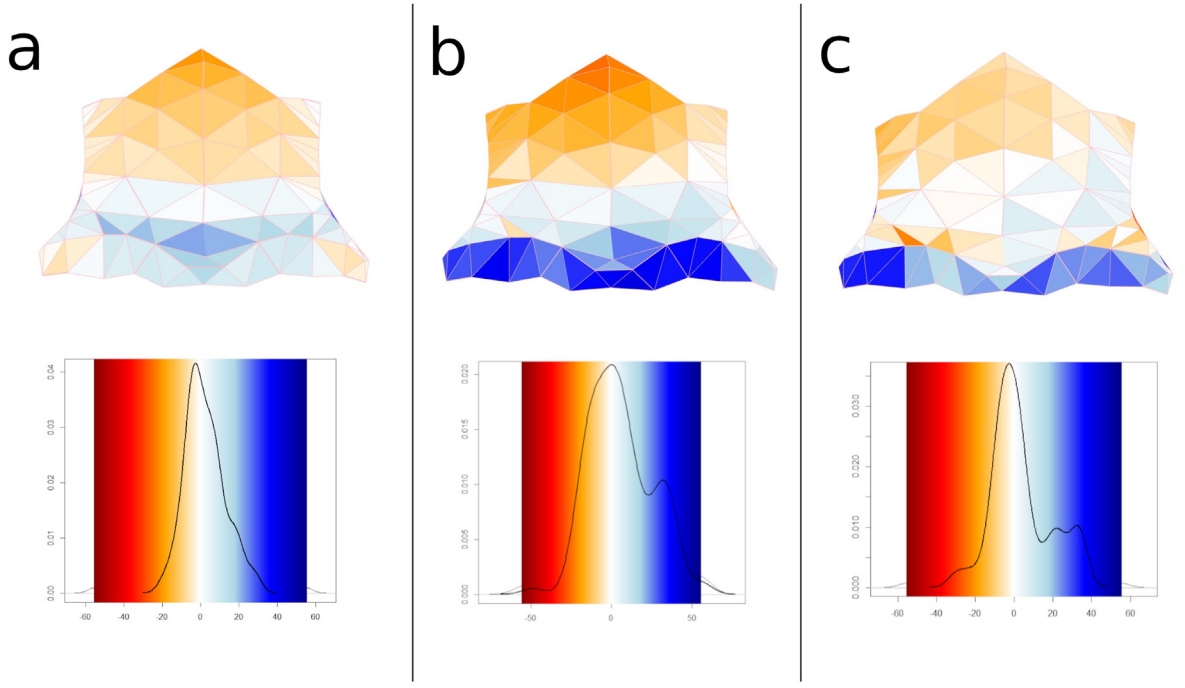

Figure 9. Three-dimensional map variations of the frontal squama showing average PC1/PC2 shape of Kocabaş compared to the average of Middle Pleistocene *Homo* (a), *Homo erectus* s.l. (b), and comparison between Middle Pleistocene *Homo* and *H. erectus* s.l. (c). Color maps are reported in frontal view. Warm and cold colors indicate respectively which regions in the average shapes are respectively locally expanded and contracted compared to Kocabaş (a, b) and in which regions in the average morphologies of *H. erectus* s.l. are respectively locally expanded and contracted compared to Middle Pleistocene *Homo* (c). Below are indicated the distributions of shape differences for each comparison. Abbreviation: PC, principal component.

slightly more expanded medial post-toral area in Kocabaş than in Middle Pleistocene *Homo*. The comparison between average *H. erectus* s.l. and Middle Pleistocene *Homo* shows a similar colormap as that between Kocabaş and *H. erectus* s.l. However, absolute local differences are less extreme than in the Kocabaş comparison as Middle Pleistocene *Homo* shows a more expanded supraorbital torus but a constricted upper frontal squama region compared to *H. erectus* s.l.

We observe a certain degree of geographical and temporal differentiation between our sampled *H. erectus* s.l. also in this plot along PC1 from older to younger specimens. Middle to Late Pleistocene East and Southeast Asian specimens tend to have positive PC1 and negative PC2 scores, closer to fossil *H. sapiens*. By vcontrast, Early Pleistocene African and Middle Pleistocene African and Eurasian fossils have negative PC1 and positive PC2 distributions.

3.2. Unweighted pair group method using arithmetic averages cluster analysis

Results of pairwise Procrustes distances between all the fossil specimens from the last analysis were used as the distance matrix for the cluster analysis. The tree generated from the UPGMA cluster analysis (Fig. 10) shows two main branches. One branch includes the more recent, Middle–Late Pleistocene fossils, and the other branch includes the older *H. erectus* s.l. specimens. Kocabaş mean reconstruction cluster with the more recent fossils and is shown as a sister branch to Middle Pleistocene *Homo* specimens. Pairwise Procrustes distances density plots are shown in Figure 11. Kocabaş exhibits the lowest pairwise Procrustes distance with Bodo; with the other Middle Pleistocene *Homo*, it shows values consistent with within-group variation. Kocabaş pairwise distances with *H. erectus* s.l. are on average higher, and some of them are more similar to values seen in the between-group distribution.

3.3. Linear discriminant analysis

The LDA classification used two groups, Middle Pleistocene *Homo* and *H. erectus* s.l. The Kocabaş reconstructions were treated as unknown. Our cross-validation analysis correctly classified 78.9% of the cases. Only four specimens were misclassified: D3444, Sambungmacan 3, Dali, and Broken Hill 1/Kabwe. These specimens had a posterior probability to belong to the opposite group of 0.59, 0.86, 0.81, and 0.52, respectively. All Kocabaş reconstructions were classified as Middle Pleistocene *Homo* with a posterior probability between 0.990 and 1.000.

4. Discussion

Our reconstruction of the frontal bone of Kocabaş has allowed for a comprehensive, quantitative analysis of its morphology. All the reconstructions in all the analyses fall outside the convex hulls of our samples on PC1 and PC2. Nevertheless, most of the reconstructions tend to plot closest to Middle Pleistocene *Homo*, especially in our last analysis. Together with results from the UPGMA cluster analysis and the classification from the LDA, our findings point to morphological similarities between Kocabaş and Middle Pleistocene *Homo*. Our results, therefore, contrast partially with those of previous works (Guipert et al., 2011; Kappelman et al., 2008; Vialet et al., 2012, 2014, 2018), which instead concluded that Kocabaş was a representative of *H. erectus* s.l., with closer affinities to the BOU-VP-2/66 Daka, UA 31, and KNM-OG 45500 specimens (Vialet et al., 2018). Our conclusion is supported by the multiple shape analyses that we conducted, which show Kocabaş's morphological similarities to the fossils in our comparative sample. Our reconstruction of Kocabaş shows a thick supraorbital torus with a large trigone area and a relatively short frontal squama compared to the supraorbital region, a relatively shallow post-toral sulcus, and a more rounded frontal profile compared to the shelf-like morphology of African *H. erectus* such as KNM-ER3773 or KNM-OG 45500. In our PCA plots, Kocabaş consistently plots between the more derived Middle Pleistocene *Homo* sample and the more archaic *H. erectus* s.l. specimens. The results of our cluster analysis and classification, in addition to Kocabaş position in the PCA plots, taken together support a closer relationship to Middle Pleistocene *Homo*.

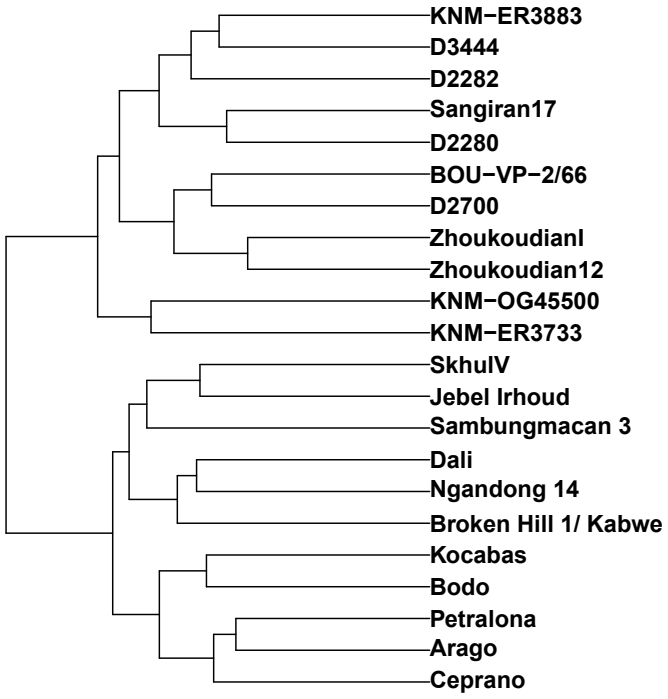

Figure 10. Unweighted pair group method using arithmetic averages cluster analysis based on pairwise Procrustes distances between individuals.

4.1. Kocabaş taxonomy and working hypotheses

Our study highlights the continuity of frontal bone shape in Africa during the Early Pleistocene. This continuum begins with the emergence of *H. erectus* s.l. diagnostic features, expressed in specimens such as KNM-ER 3733, and lasts up to about 1 Ma, represented in our study by the KNM-OG 45500 and BOU-VP-2/66 Daka specimens. Beginning in the Middle Pleistocene, some fossils show a more derived morphology. Our results show this to the extent that Middle to Late Pleistocene fossils across Africa and Eurasia are distinct from the Early Pleistocene fossils along the major axis of variation in shape space (i.e., along PC1 and PC2 in Fig. 8; for a more detailed discussion about frontal shape variation see also Mori et al., 2020), consistent with previous GM studies on cranial forms (Manzi et al., 2003; Baab, 2015, 2016; Manzi, 2016; Profico et al., 2016). The UPGMA phenogram (Fig. 9) also shows two temporal clusters that split our fossil sample primarily by chronology, from early specimens dated to between ca. 1.77 to 0.7 Ma to more derived specimens dated to the Middle and Late Pleistocene. These observations suggest a taxonomic and phylogenetic discontinuity that ranges across the Matuyama/Brunhes reversal of 780 ka, in a possible relationship with the more general phenomenon known as the 'Mid-Pleistocene revolution' (Maslin and Ridgwell, 2005) that, in turn, corresponds to the beginning of environmental changes of Marine Isotope Stages 18–16, and to the time period when the common ancestor of the *H. sapiens*, *H. neanderthalensis* and Denisovan lineages is thought to have emerged (e.g., Bergström et al., 2021). Phenetic differences between Early and Middle Pleistocene fossils might represent a distinction at the species level in our analyses. Unfortunately, a gap in fossil evidence between 1 Ma and 600 ka makes it difficult to track evolutionary changes in the genus *Homo* in this period. However, after this time, more encephalized hominins were widespread in Africa and Eurasia.

The systematics of Middle Pleistocene *Homo* are highly contested and remain unresolved. Disagreement exists over the number and nomina of taxa that should be recognized, as well as their potentially ancestral status to *H. neanderthalensis* and *H. sapiens*. (Rightmire, 2008, 2009; Hublin, 2009; Mounier et al., 2009; Mounier et al., 2011; Stringer, 2012; Grün et al., 2020; Harvati and Reyes-Centeno, 2022; Roksandic et al., 2022). In light of the current debate and the uncertainty on Middle Pleistocene *Homo*

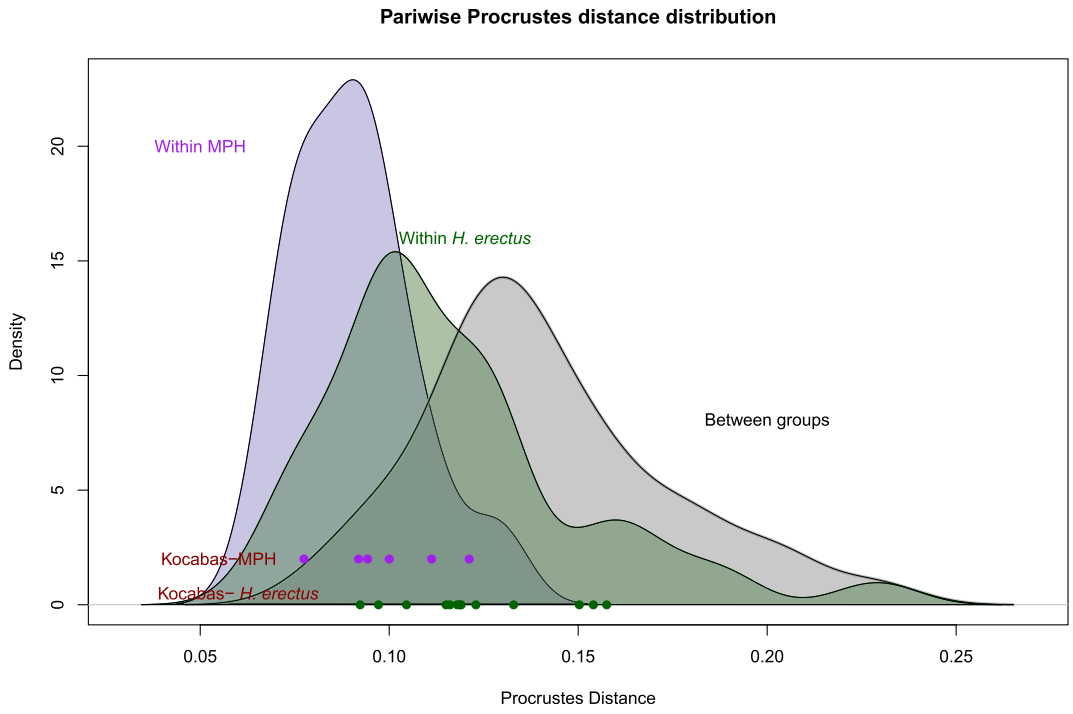

Figure 11. Pairwise Procrustes distances density plot in Middle Pleistocene *Homo* (purple) and *Homo erectus* s.l. (green) and between the two groups (gray). Pairwise Procrustes distances of Kocabaş with specimens belonging to Middle Pleistocene *Homo* and *H. erectus* s.l. are reported under the density lines.

systematic, it is difficult to address the taxonomy of Kocabaş. However, we feel that Kocabaş may be an early representative of the same taxonomic unit to which Bodo, Borken Hill 1/Kabwe, and Ceprano belong, given the morphological similarities it shows to these fossils. These specimens are often attributed to *H. heidelbergensis* s.l. (Rightmire, 1996, 2013, 2015; Schwartz and Tattersall, 1996; Tattersall, 2000; Stringer, 2002; Mounier et al., 2011; Di Vincenzo et al., 2017). More recently, these fossils have been proposed as part of the hypodigm of *H. bodoensis* (Roksanic et al. 2022). Future research should focus on clarifying these relationships. However, our analysis shows that Kocabaş does not show typical *H. erectus* s.l. frontal bone morphology and that instead it could represent a different taxon, which was widespread in Africa and Eurasia during the Middle Pleistocene. The proposed chronology of the Kocabaş specimen would make it the earliest currently known representative of this taxon: the paleomagnetic and cosmogenic nucleotide study of the travertine quarry from which the specimen originates proposed an age for Kocabaş between 1.0 and 1.5 Ma (Lebatard et al., 2014), with the later limit considered more plausible. The Levantine corridor, which is close to Kocabaş geographic location, has been suggested as a place inhabited by a 'source population,' which may have given rise to new taxa between the Early and Middle Pleistocene (Bermùdez de Castro and Martinón-Torres, 2013). Therefore, Kocabaş in its geographic location in the Eastern Mediterranean could reasonably be an early member of a species, potentially *H. heidelbergensis* s.l., which may also represent the most recent common ancestor of the three subsequent Pleistocene human lineages (*H. sapiens*, *H. neanderthalensis*, and Denisovans) in Africa, Europe, and Asia, respectively. Such geographical position and morphology, which is not as derived as the other Middle Pleistocene *Homo* but it is less plesiomorphic than African *H. erectus,* also represents a link between the Early Pleistocene African populations and the subsequent Middle Pleistocene Eurasian *Homo* forms. At present, we have little evidence regarding other possible candidates representing early forms of *H. heidelbergensis* s.l. Other possible candidates for an early form of *H. heidelbergensis* s.l. are the Gombore MK 1 and MK 2 cranial fragments from Ethiopia (Profico et al., 2016), dated around 850 ka, and therefore postdating the proposed age of Kocabaş. Unfortunately, the preservation of Gombore precludes a direct comparison with Kocabaş. BOU-VP-2/66 Daka fossil was also suggested to have morphological affinities to Middle Pleistocene *Homo,* such as Boken Hill 1/Kabwe (Baab, 2016). In our analysis, BOU-VP-2/66 Daka exhibit a frontal morphology not far from that of Boken Hill 1/Kabwe in PC1 PC2 plot (Fig. 8), with a more derived (PC1) morphology than that of other Early Pleistocene African *H. erectus,* and a PC2 score similar to the Broken Hill 1/Kabwe specimen. However, in our analysis of frontal bone morphology, overall Procrustes distances place this specimen closer to *H. erectus* s.l. However, our dataset, which only comprises frontal bone landmarks and semilandmarks due to the state of preservation of the Kocabaş specimen, it does not include other pertinent morphological features highlighted by Baab (2016) that could link BOU-VP-2/66 Daka to other Middle Pleistocene *Homo* fossil (e.g., more vertical parietal morphology, vertical occipital plane, or high arched temporal squama).

Overall, taken together, these specimens may represent the earliest forms of this new geographically widespread taxon.

Another possibility is that Kocabaş represents a geographic variety of *H. erectus* s.l. and that differences from other *H. erectus* s.l. individuals represent intraspecific differences among paleodemes of this widespread taxon. Testing such a hypothesis is difficult, given the limited fossil record from this geographic area and timeframe. The only temporally comparable specimens in our sample, OH 9, BOU-VP-2/66 Daka, and KNM-OG 45500 (Leakey, 1971; Asfaw et al., 2002; Potts et al., 2004), differ from Kocabaş in their frontal bone shape. Overall, Kocabaş is more similar in frontal bone morphology to Middle Pleistocene specimens in our analysis, although it also shares some similarities with specimens dating to the end of the Early Pleistocene. When compared to OH 9, Kocabaş

shows similar PC2 scores (thick supraorbital torus) but differs in its PC1 score (less marked post-toral sulcus and post-orbital constriction), which represents most of the variance in our analysis. Moreover, this comparison does not take into account important aspects of the frontal morphology missing in OH 9, whose lack of preservation of the bregma area prevents an evaluation of overall frontal bone height. However, this feature is fundamental when evaluating more or less derived morphology, as shown in our other results. Overall, this hypothesis would be supported only if we accept an even greater variability for *H. erectus s.l.* than commonly recognized—which would also imply that later African fossils such as Broken Hill 1/Kabwe and Bodo should be assigned to this taxon, an implication that currently we do not support.

A third possibility is that Kocabaş is younger than the currently proposed chronology. The history of this specimen makes it hard to be certain about its stratigraphic position and the context of its recovery (Vialet et al., 2012; Lebatard et al., 2014; Aytek and Harvati, 2016). Its dating has been a difficult task, which has produced a range of results. The first dating attempts placed it around 400 ka (uranium-thorium analysis) and 500 ka (thermoluminescence method; Altunel, 1996; Kappelman et al., 2008). A subsequent study based on electron spin resonance (ESR) dating (of calcite collected in the basin) proposed a much earlier age of 1.1 Ma (Engin et al., 1999). Most recently, paleomagnetic and cosmogenic nucleotide studies placed it even earlier to around 1 to 1.5 Ma (Lebatard et al., 2014). A last analysis based on the U/Th dating of the travertine yelded an age older than 0.55–1.31 Ma (Claes et al., 2020). None of these studies dated the hominin specimen directly. The paleontological remains (recovered from different blocks from the mine) are also scarce and poorly studied. Erten and colleagues (Erten et al., 2005) concluded that the faunal remains were “insufficient to propose any reliable date” (Erten et al., 2005: 276), although the *Equus* specimens might agree with the previously proposed age of 400 Ka. In contrast, a later study by Boulbes et al. (2014) considered them compatible with the Villafranchian faunal assemblage and concluded that they could be older than 1.2 Ma. These widely diverging age estimates, combined with the history of discovery of the Kocabaş specimen during mining operations and not in controlled archaeological excavation, and its lack of secure context, have led to the questioning of the validity of its proposed very ancient geological age (Muttoni et al., 2018). Caution should be exercised when evaluating the potential geological age of a fossil specimen based on its morphology (e.g., Berger et al., 2015, 2017). However, a later, early Middle Pleistocene geological age for Kocabaş would be more consistent with its morphological affinities with Middle Pleistocene *Homo* found in our analyses.

4.2. Comparison with previous work and reconstruction bias

Compared to the earlier published analyses of the Kocabaş specimen, we found some similarities and differences in our results. Our findings agree with those of the geometric morphometric shape analysis presented by Vialet et al. (2014) in the way that both place Kocabaş close to Broken Hill/Kabwe and Bodo but differ with their conclusions, and those of more recent work by those authors (Vialet et al., 2018), who concluded that Kocabaş represents and African *H. erectus* s.l. specimen. We agree with Aytek and Harvati (2016) in confirming some of the differences those authors observed between OH 9 and Kocabaş, as well as with their finding of affinities between Kocabaş and Middle Pleistocene *Homo*. However, contrary to that more limited study, we did not find Kocabaş to be closer to Chinese *H. erectus* in shape space.

Aytek and Harvati (2016) interpreted the results of Vialet et al. (2014) as influenced by a lack of coverage of the supraorbital area in the landmark set. In contrast, Vialet et al. (2018) argued that the results of Aytek and Harvati (2016) were driven by a landmark configuration that focused solely on the supraorbital region. To overcome this problem, we quantified and analyzed the morphology of the frontal bone in its totality, comprising information from both the supraorbital torus and the frontal squama. Our study shows that the frontal bone shape differences between earlier *H. erectus* and Middle Pleistocene *Homo* are related to the multivariate pattern of shape differences in both supraorbital morphology and frontal squama relative size and shape. Furthermore, our results show that the Kocabaş frontal bone morphology is intermediate between African/Georgian *H. erectus* s.l. and Middle Pleistocene African *Homo,* with closer affinities to the latter. Our findings, therefore, contrast with those of Vialet et al. (2014, 2018), who concluded that Kocabaş represents African *H. erectus s.l.*

Some of the differences between our results and those of Vialet et al. (2018) could be related to differences in the reconstruction steps as the alignment of disarticulated fragments is difficult to reproduce and is subject to inter and intraindividual error (Weber, 2015). For this reason, we performed two alignments and two mirroring procedures (using two different methods, see Material and Methods) and multiple reconstructions of the missing areas, so as to mitigate this source of error. TPS alignment of mirrored parts is less subjective than the manual alignment, and it is considered to better represent the morphology of the original specimen (Benazzi and Senck, 2011). Therefore, we consider the Kocabaş 2 reconstruction as more precise/reproducible. We could not directly test how much our reconstructions differ from the ones produced by Vialet and colleagues. However, our results show that even two different alignments made by the same observer (T.M.) give slightly different results in the GM analysis (see PCA plots). Differences between the two alignments and the mirroring step are clearly shown in the second analysis (Fig. 6), which was based on the dataset derived only from the preserved portion of fossils. Therefore, differences between the two reconstructions in this plot are mainly the result of intraobserver error in the alignment and the different mirroring steps since landmark precision was shown to be high in our error test. Although the two reconstructions differ somewhat in their PC 1 and 2 scores, these differences do not affect their position relative to the comparative samples and, therefore, the interpretation of the results. Additionally, the reconstruction of the missing areas of the frontal squama and the medial aspect of the supraorbital torus was substantial and was obtained using different reference samples, including a wide geographical and temporal range of *H. erectus* s.l. specimens, as well as the Petralona cranium. These reference specimens differ in their supraorbital torus morphology, ranging from an extremely double-arched shape, as seen in BOU-VP-2/66 Daka, to a more straight shape, as shown by Sambungmacan 3. They also differ in frontal squama shape, ranging from more elongated to more rounded morphologies. When assessing the results from our different datasets, our PCA plots show that the multiple Kocabaş reconstructions had similar PC1/PC2 scores, despite the differences in the reference samples. We therefore conclude that the reference specimens did not influence the position of Kocabaş in our analyses or our interpretations of this specimen's morphology.

Compared to the analyses by Vialet et al. (2018) our work also differs in the datasets and types of analyses used. In contrast to the geometric morphometric analysis which captures the shape of the frontal bone, Vialet et al. (2018) conducted a multivariate analysis of four linear frontal bone measurements. In addition to the difference in the number of variables used, their variables were not size-corrected; therefore, the PCA plot derived from their dataset is most probably influenced by differences in size. As stated already in the introduction, the lack of size correction signifies that

the first PC of their PCA captures mainly differences in overall size. Vialet et al. (2018) considered the first component to be informative from a phylogenetic point of view. However, size differences are generally considered less informative on phylogenetic relationships than shape differences, captured in a geometric morphometric analysis. In their cladistic analysis, Vialet et al. (2018) did not include any Middle Pleistocene specimens, even though affinities between Kocabaş and Middle Pleistocene *Homo* had already been noted (Kappelman et al., 2008; Vialet et al., 2014; Aytek and Harvati, 2016). Therefore, in that analysis, they did not evaluate the relationship between Kocabaş and Middle Pleistocene *Homo* or test the competing hypothesis to their conclusion (i.e., that Kocabaş represents Middle Pleistocene *Homo* taxon rather than *H. erectus* s.l.). In our analysis, therefore, we wanted to directly test phenetic similarities of Kocabaş frontal morphology with a comparative sample of *H. erectus* s.l. and Middle Pleistocene *Homo* in order to address the limitations highlighted in these previous works.

4.3. Limitations and future directions

This study relied on the virtual reconstruction of an incomplete specimen, which introduces a level of uncertainty, even if we tried to reduce the error related to this procedure by producing multiple reconstructions and by analyzing different datasets, including one comprising only the preserved aspects of the fossil. At present, it is clear that the manual alignment of the fragments is difficult to replicate, and therefore, it is important to find new automatic approaches to accomplish this step (see Profico et al., 2019), even if the associated error is small.

Future work should focus on reassessing the geological age of the specimen, perhaps attempting the direct dating of the hominin fossil itself, to resolve lingering questions about its lack of geological and stratigraphic context and the circumstances of its discovery outside controlled excavation. A more firmly established age for the Kocabaş specimen would allow the evaluation of this important specimen in the proper comparative and evolutionary framework. Regarding the morphometric analysis, future work should aim to investigate Neanderthal frontal morphology in relation to Kocabaş and the other Middle Pleistocene *Homo* specimens. In our study, including *H. sapiens* helped evaluate both more plesiomorphic and more derived morphology in frontal bone shape (PC1 axes of separation). However, it is important to note that *H. sapiens*, with its highly derived morphology, polarized the shape space in our analyses. We mitigated the influence of modern humans in our final shape analysis when we removed them from the sample. The current work did not include any Neanderthals as our aim was to test morphological similarities of Kocabaş frontal bone to *H. erectus* s.l. and Middle Pleistocene *Homo*. However, including Neanderthals in future studies could provide additional information regarding the potential polarity of the shape features found in the Kocabaş frontal bone.

Our analyses also produced some results regarding OH 9 that might be worth further consideration. In our analyses, OH 9 plots in a separate position compared to other Early Pleistocene African *H. erectus* s.l. specimens. Overall, in PC1, OH 9 has a very low value, similar to the more archaic African specimens. PC2, on the other hand, shows a more derived morphology, more similar to later Middle Pleistocene *Homo* and Asian *H. erectus*. In this context, given the limited amount of data taken on OH 9 and the focus of our analysis on maximizing the shape variables from Kocabaş, we think that this result alone is not enough for addressing open taxonomic questions about this specimen. However, future research should aim to further investigate this important specimen using virtual anthropology and geometric morphometrics approaches.

5. Conclusions

Our analyses highlighted the presence in Kocabaş of some features typical of later Middle Pleistocene *Homo*, such as a big supraorbital torus associated with a relatively short frontal squama. Together with cluster analysis and LDA classification procedure, Kocabaş seems to be part of the same taxonomic unit, which comprises Eurasian (Ceprano) and African (Bodo and Broken Hill 1/Kabwe) specimens. We consider different evolutionary hypotheses, but following our results, we conclude that Kocabaş most likely does not belong to *H. erectus* s.l. Future work should aim to provide a more reproducible reconstruction, less influenced by the manual alignment step. Moreover, the proposed geological age of this specimen should be further assessed and evaluated. In conclusion, our results refute previous analyses, which placed this specimen in the *H. erectus* s.l. hypodigm, instead we propose that Kocabaş is a member of Middle Pleistocene *Homo* taxon usually described as *H. heidelbergensis* s.l.

CRediT authorship contribution statement

Tommaso Mori: Conceptualization, Data curation, Formal analysis, Investigation, Methodology, Project administration, Software, Validation, Visualization, Writing – original draft, Writing – review & editing. **Alessandro Riga:** Formal analysis, Methodology, Supervision, Visualization, Writing – review & editing, Validation. **Ahmet Ihsan Aytek:** Data curation, Writing – review & editing, Investigation, Resources. **Katerina Harvati:** Conceptualization, Data curation, Formal analysis, Funding acquisition, Investigation, Methodology, Project administration, Resources, Software, Supervision, Validation, Writing – review & editing.

Acknowledgments

K.H. is supported by the European Research Council (ERC CoG 724703 'CROSSROADS'; ERC AdG 101019659 'FIRSTSTEPS') and the Deutsche Forschungsgemeinschaft (DFG FOR 2237). T.M. is supported by project grant DiVInA (UNIFI_FSC2022) funded by Regione Toscana and Sistema Museale di Ateneo University of Florence. A.R was supported by the Italian Ministry of University and Research (MUR, PRIN project 2022): grant no. 2022KJB743. We thank the following institutions and colleagues for access to fossil comparative material: Richard Potts and colleagues at the Smithsonian Institution, as well as FredrickManthi, Timothy Gichunge, and the members of the Department of Earth Science, National Museums of Kenya for access to the KNM-OG 45500 surface scan and computed tomography (CT) scans of KNM-ER 3733 and KNM-ER 3883; Gen Suwa, the Authority for Research and Conservation of Cultural Heritage (ARCCH), and the National Museum of Ethiopia for providing the Daka calvarium (BOU-VP-2/66 Daka) external mesh reconstruction; Sabine Eggers for access to CT scan from the Department of Anthropology of the Naturhistorisches Museum in Vienna; Philipp Gunz for sharing of the Arago recontruction; Giselle Garcia and Eric Delson, American Museum of Natural History; Monica Zavattaro, Fabio Di Vincenzo and JacopoMoggi-Cecchi for access to the CT scans from the Anthropological Collection at the Museo di Storia Naturale dell' Università di Firenze; Antoine Balzeau, Martin Friess, and Dominique Grimaud-Hervé for access to the CT scans from the Muséum national d'Histoire naturelle, Paris. The Skhūl V fossil scan was downloaded from the Peabody Museum, Harvard University, while the *H. naledi* (DH1 and DH3) scans were downloaded from the MorphoSource database, Duke University (media number: M7300-8170). We thank Marlijn Noback for providing access to scans of the modern human comparative sample, as well as YonatanSahle for facilitating access

to the Daka CT. Finally, we thank HannesRathmann for his help with the figures' production.

Supplementary Online Material

Supplementary Online Material to this article can be found online at https://doi.org/10.1016/j.jhevol.2024.103517.

References

Altunel, E., 1996. Pamukkale travertenlerinin morfolojiközellikleri, yaşları ve neotektonikönemleri. MTA dergisi 118, 47–64.

Asfaw, B., Gilbert, W.H., Beyene, Y., Hart, W.K., Renne, P.R., WoldeGabriel, G., Vrba, E.S., White, T.D., 2002. Remains of *Homo erectus* from Bouri, Middle Awash, Ethiopia. Nature 416, 317.

Aytek, A.İ., Harvati, K., 2016. The human fossil record from Turkey. In: Harvati, K., Roksandic, M. (Eds.), Paleoanthropology of the Balkans and Anatolia. Springer, Dordrecht, pp. 79–91.

Baab, K.L., 2015. Defining *Homo erectus*. In: Henke, W., Tattersall, I. (Eds.), Handbook of Paleoanthropology, 2nd ed. Springer, Berlin, pp. 2189–2219.

Baab, K.L., 2016. The role of neurocranial shape in defining the boundaries of an expanded *Homo erectus* hypodigm. J. Hum. Evol. 92, 1–21.

Baab, K.L., Rogers, M., Bruner, E., Semaw, S., 2022. Reconstruction and analysis of the DAN5/P1 and BSN12/P1 Gona early Pleistocene *Homo* fossils. J. Hum. Evol. 162, 103102.

Benazzi, S., Senck, S., 2011. Comparing 3–dimensional virtual methods for reconstruction in craniomaxillofacial surgery. J. Oral Maxillofac. Surg. 69, 1184–1194.

Bermùdez de Castro, J.M., Martinón-Torres, M., 2013. A new model for the evolution of the human Pleistocene populations of Europe. Quat. Int. 295, 102–112.

Berger, L.R., Hawks, J., de Ruiter, D.J., Churchill, S.E., Schmid, P., Delezene, L.K., Kivell, T.L., Garvin, H.M., Williams, S.A., DeSilva, J.M., 2015. *Homo naledi*, a new species of the genus *Homo* from the Dinaledi Chamber, South Africa. eLife 4, e09560.

Berger, L.R., Hawks, J., Dirks, P.H., Elliott, M., Roberts, E.M., 2017. *Homo naledi* and Pleistocene hominin evolution in subequatorial Africa. eLife 6, e24234.

Bergström, A., Stringer, C., Hajdinjak, M., Scerri, E.M., Skoglund, P., 2021. Origins of modern human ancestry. Nature 590, 229–237.

Black, D., 1931. On an adolescent skull of *Sinanthropus pekinensis* in comparison with an adult skull of the same species and with other hominid skulls, recent and fossil. Paleontol. Sin. D 7, 1–144.

Bookstein, F.L., 1989. Principal warps: thin-plate splines and the decomposition of deformations. IEEE Trans. Pattern Anal. Mach. Intell. 11, 567–585.

Bookstein, F.L., 1991. Morphometric Tools for Landmark Data: Geometry and Biology. Cambridge University Press, Cambridge.

Bookstein, F.L., 1997. Morphometric Tools for Landmark Data: Geometry and Biology. Cambridge University Press, Cambridge.

Bosman, A., Buck, L., Reyes-Centeno, H., Mirazón Lahr, M., Stringer, C., Harvati, K., 2019. The Kabua I cranium: virtual anatomical reconstructions. In: Sahle, Y., Reyes-Centeno, H., Bentz, C. (Eds.), Modern Human Origins and Dispersal. Kerns Verlag, Tuebingen, pp. 137–170.

Bosman, A.M., Reyes-Centeno, H., Harvati, K., 2020. A virtual assessment of the suprainiac depressions on the Eyasi I (Tanzania) and Aduma ADU-VP-1/3 (Ethiopia) Pleistocene hominin crania. J. Hum. Evol. 145, 102815.

Boulbes, N., Mayda, S., Titov, V.V., Alçiçek, M.C., 2014. Les grands mammifères du Villafranchien supérieur des travertins du Bassin de Denizli (Sud-Ouest Anatolie, Turquie). L'Anthropologie 118, 44–73.

Buck, L.T., Stringer, C.B., 2015. A rich locality in South Kensington: The fossil hominin collection of the Natural History Museum, London. Geol. J. 50, 321–337.

Carbonell, E., Bermudez de Castro, J.M., Parés, J.M., Pérez-González, A., Cuenca-Bescós, G., Ollé, A., Mosquera, M., Huguet, R., Van Der Made, J., Rosas, A., 2008. The first hominin of Europe. Nature 452, 465–469.

Claes, H., Török, Á., Soete, J., Mohammadi, Z., Vassilieva, E., Hamaekers, H., Erthal, M.M., Aratman, C., Cheng, H., Edwards, R.L., Shen, C., Özkul, M., Kele, S., Mindszenty, A., Swennen, R., 2020. U/Th dating and open system behavior: implications for travertines based on the study of Süttő (Hungary) and Ballik (Turkey) sites. Quaternaire 31, 117–132.

Di Vincenzo, F., Profico, A., Bernardini, F., Cerroni, V., Dreossi, D., Schlager, S., Zaio, P., Benazzi, S., Bidditu, I., Rubini, M., Tunic, C., Manzi, G., 2017. Digital reconstruction of the Ceprano calvarium (Italy), and implications for its interpretation. Sci. Rep. 7, 13974.

Engin, B., Güven, O., Köksal, F., 1999. Electron spin resonance age determination of a travertine sample from the southwestern part of Turkey. Appl. Radiat. Isot. 51, 689–699.

Erten, H., Sen, S., Özkul, M., 2005. Pleistocene mammals from travertine deposits of the Denizli basin (SW Turkey). Ann. Paleontol. 91, 267–278.

Falguères, C., Shao, Q., Han, F., Bahain, J., Richard, M., Perrenoud, C., Moigne, A., 2015. New ESR and U-series dating at Caune de l'Arago, France: A key-site for European Middle Pleistocene. Quat. Geochronol. 30, 547–553.

Field, A., 2013. Discovering Statistics Using IBM SPSS Statistics, Fourth ed. Sage, London.

Gabunia, L., Vekua, A., 1995. A Plio-Pleistocene hominid from Dmanisi, East Georgia, Caucasus. Nature 373, 509.

Garcia, T., Féraud, G., Falguères, C., de Lumley, H., Perrenoud, C., Lordkipanidze, D., 2010. Earliest human remains in Eurasia: New $^{40}Ar/^{39}Ar$ dating of the Dmanisi hominid-bearing levels, Georgia. Quat. Geochronol. 5, 443–451.

Gower, J.C., 1975. Generalized Procrustes analysis. Psychometrika 40, 33–51.

Grün, R., 1996. A re-analysis of electron spin resonance dating results associated with the Petralona hominid. J. Hum. Evol. 30, 227–241.

Grün, R., 2006. Direct dating of human fossils. Am. J. Phys. Anthropol. 131, 2–48.

Grün, R., Pike, A., McDermott, F., Eggins, S., Mortimer, G., Aubert, M., Kinsley, L., Joannes-Boyau, R., Rumsey, M., Denys, C., 2020. Dating the skull from Broken Hill, Zambia, and its position in human evolution. Nature 580, 372–375.

Grün, R., Stringer, C.B., 1991. Electron spin resonance dating and the evolution of modern humans. Archaeometry 33, 153–199.

Guipert, G., Vialet, A., Alcicek, M.C., 2011. The *Homo erectus* from Kocabaş in Turkey and the first settlements in Eurasia. Am. J. Phys. Anthropol. 144 (Suppl. 52), 151.

Gunz, P., Mitteroecker, P., Bookstein, F.L., 2005. Semilandmarks in three dimensions. In: Slice, D.E. (Ed.), Modern Morphometrics in Physical Anthropology. Springer, Boston, pp. 73–98.

Gunz, P., Mitteroecker, P., Neubauer, S., Weber, G.W., Bookstein, F.L., 2009. Principles for the virtual reconstruction of hominin crania. J. Hum. Evol. 57, 48–62.

Harvati, K., Hublin, J.-J., Gunz, P., 2010. Evolution of Middle-Late Pleistocene human cranio-facial form: A 3-D approach. J. Hum. Evol. 59, 445–464.

Harvati, K., Reyes-Centeno, H., 2022. Evolution of *Homo* in the Middle and Late Pleistocene. J. Hum. Evol. 173, 103279.

Hublin, J.-J., 2009. The origin of Neandertals. Proc. Natl. Acad. Sci. USA 106, 16022–16027.

Kappelman, J., Alçiçek, M.C., Kazancı, N., Schultz, M., Özkul, M., Şen, Ş., 2008. First *Homo erectus* from Turkey and implications for migrations into temperate Eurasia. Am. J. Phys. Anthropol. 135, 110–116.

Khatib, S., Rochette, P., Alçiçek, M.C., Lebatard, A.-E., Demory, F., Saos, T., 2014. Études stratigraphique, sédimentologique et paléomagnétique des travertins de Kocabaş, Bassin de Denizli, Anatolie, Turquie, contenant des restes fossiles quaternaires. L'Anthropologie 118, 16–33.

Lachenbruch, P.A., Goldstein, M., 1979. Discriminant analysis. Biometrics 35, 69–85.

Larick, R., Ciochon, R.L., Zaim, Y., Rizal, Y., Aziz, F., Reagan, M., Heizler, M., 2001. Early Pleistocene $^{40}Ar/^{39}Ar$ ages for Bapang Formation hominins, central Jawa, Indonesia. Proc. Natl. Acad. Sci. USA 98, 4866–4871.

Leakey, M.D., 1971. Olduvai Gorge: Volume 3, Excavations in Beds I and II, 1960–1963. Cambridge University Press, Cambridge.

Lebatard, A.-E., Alçiçek, M.C., Rochette, P., Khatib, S., Vialet, A., Boulbes, N., Bourlès, D.L., Demory, F., Guipert, G., Mayda, S., 2014. Dating the *Homo erectus* bearing travertine from Kocabaş (Denizli, Turkey) at least 1.1 Ma. Earth Planet. Sci. Lett. 390, 8–18.

Lepre, C.J., Kent, D.V., 2015. Chronostratigraphy of KNM-ER 3733 and other area 104 hominins from Koobi Fora. J. Hum. Evol. 86, 99–111.

Manzi, G., 2016. Humans of the Middle Pleistocene: The controversial calvarium from Ceprano (Italy) and its significance for the origin and variability of *Homo heidelbergensis*. Quat. Int. 411, 254–261.

Manzi, G., Bruner, E., Passarello, P., 2003. The one-million-year-old *Homo* cranium from Bouri (Ethiopia): A reconsideration of its *H. erectus* affinities. J. Hum. Evol. 44, 731–736.

Manzi, G., Magri, D., Milli, S., Palombo, M.R., Margari, V., Celiberti, V., Barbieri, M., Barbieri, M., Melis, R.T., Rubini, M., 2010. The new chronology of the Ceprano calvarium (Italy). J. Hum. Evol. 59, 580–585.

Maslin, M.A., Ridgwell, A.J., 2005. Mid-Pleistocene revolution and the 'eccentricity myth'. Geol. Soc. Spec. Publ. 247, 19–34.

Matsu'ura, S., Kondo, M., Danhara, T., Sakata, S., Iwano, H., Hirata, T., Kurniawan, I., Setiyabudi, E., Takeshita, Y., Hyodo, M., 2020. Age control of the first appearance datum for Javanese *Homo erectus* in the Sangiran area. Science 367, 210–214.

McDougall, I., Brown, F.H., Vasconcelos, P.M., Cohen, B.E., Thiede, D.S., Buchanan, M.J., 2012. New single crystal $^{40}Ar/^{39}Ar$ ages improve time scale for deposition of the Omo group, Omo–Turkana Basin, East Africa. J. Geol. Soc. 169, 213–226.

Mitteroecker, P., Bookstein, F., 2011. Linear discrimination, ordination, and the visualization of selection gradients in modern morphometrics. Evol. Biol. 38, 100–114.

Mitteroecker, P., Gunz, P., 2009. Advances in geometric morphometrics. Evol. Biol. 36, 235–247.

Mori, T., Profico, A., Reyes-Centeno, H., Harvati, K., 2020. Frontal bone virtual reconstruction and geometric morphometric analysis of the mid-Pleistocene hominin KNM-OG 45500 (Olorgesailie, Kenya). J. Anthropol. Sci. 98, 49–72.

Mounier, A., Condemi, S., Manzi, G., 2011. The stem species of our species: A place for the archaic human cranium from Ceprano, Italy. PLoS One 6, e18821.

Mounier, A., Marchal, F., Condemi, S., 2009. Is *Homo heidelbergensis* a distinct species? New insight on the Mauer mandible. J. Hum. Evol. 56, 219–246.

Muttoni, G., Scardia, G., Kent, D.V., 2018. Early hominins in Europe: The Galerian migration hypothesis. Quat. Sci. Rev. 180, 1–29.

Noback, M.L., Harvati, K., 2014. Covariation in the human masticatory apparatus. Anat. Rec. 298, 64–84.

Noback, M.L., Harvati, K., 2015. The contribution of subsistence to global human cranial variation. J. Hum. Evol. 80, 34–50.

Nomade, S., Muttoni, G., Guillou, H., Robin, E., Scardia, G., 2011. First $^{40}Ar/^{39}Ar$ age of the Ceprano man (central Italy). Quat. Geochronol. 6, 453–457.

Potts, R., Behrensmeyer, A.K., Deino, A., Ditchfield, P., Clark, J., 2004. Small mid-Pleistocene hominin associated with East African Acheulean technology. Science 305, 75–78.

Profico, A., Buzi, C., Davis, C., Melchionna, M., Veneziano, A., Raia, P., Manzi, G., 2019. A new tool for digital alignment in virtual anthropology. Anat. Rec. 302, 1104–1115.
Profico, A., Buzi, C., Castiglione, S., Melchionna, M., Piras, P., Veneziano, A., Raia, P., 2021. Arothron: an R package for geometric morphometric methods and virtual anthropology applications. Am. J. Phys. Anthropol. 176, 144–151.
Profico, A., Buzi, C., Di Vincenzo, F., Boggioni, M., Borsato, A., Boschian, G., Marchi, D., Micheli, M., Moggi-Cecchi, J., Samadelli, M., Tafuri, M.A., Arsuaga, J.L., Manzi, G., 2023. Virtual excavation and analysis of the early Neanderthal cranium from Altamura (Italy). Commun. Biol. 6, 316.
Profico, A., Di Vincenzo, F., Gagliardi, L., Piperno, M., Manzi, G., 2016. Filling the gap. Human cranial remains from Gombore II (Melka Kunture, Ethiopia; ca. 850 ka) and the origin of *Homo heidelbergensis*. J. Anthropol. Sci. 94, 1–24.
Profico, A., Veneziano, A., Melchionna, M., Piras, P., Raia, P., 2018. Arothron: R functions for geometric morphometrics analyses. R package version 1.1.
R Core Team, 2021. R: A Language and Environment for Statistical Computing. R Foundation for Statistical Computing, Vienna. URLhttps://www.R-project.org/.
Richter, D., Grün, R., Joannes-Boyau, R., Steele, T.E., Amani, F., Rué, M., Fernandes, P., Raynal, J.-P., Geraads, D., Ben-Ncer, A., Hublin, J.-J., McPherron, S.P., 2017. The age of the hominin fossils from Jebel Irhoud, Morocco, and the origins of the Middle Stone age. Nature 546, 293.
Rightmire, G.P., 2008. *Homo* in the Middle Pleistocene: Hypodigms, variation, and species recognition. Evol. Anthropol. 17, 8–21.
Rightmire, G.P., 2009. Middle and later Pleistocene hominins in Africa and Southwest Asia. Proc. Natl. Acad. Sci. USA 106, 16046–16050.
Rightmire, G.P., 2013. Homo erectus and Middle Pleistocene hominins: Brain size, skull form, and species recognition. J. Hum. Evol. 65, 223–252.
Rightmire, G.P., 2015. Later Middle Pleistocene *Homo*. In: Henke, W., Tattersall, I. (Eds.), Handbook of Paleoanthropology. Springer, Berlin, pp. 2221–2242.
Rightmire, P.G., 1996. The human cranium from Bodo, Ethiopia: Evidence for speciation in the Middle Pleistocene? J. Hum. Evol. 31, 21–39.
Rizal, Y., Westaway, K.E., Zaim, Y., van den Bergh, G.D., Bettis, E.A., Morwood, M.J., Huffman, O.F., Grun, R., Joannes-Boyau, R., Bailey, R.M., Sidarto, Westaway, M.C., Kurniawan, I., Moore, M.W., Storey, M., Aziz, F., Suminto, Zhao, J.X., Aswan, Sipola, M.E., Larick, R., Zonneveld, J.P., Scott, R., Putt, S., Ciochon, R.L., 2020. Last appearance of *Homo erectus* at Ngandong, Java, 117,000–108,000 years ago. Nature 577, 381–385.
Rohlf, F.J., Slice, D., 1990. Extensions of the Procrustes method for the optimal superimposition of landmarks. Syst. Biol. 39, 40–59.
Roksandic, M., Radović, P., Wu, X.-J., Bae, C.J., 2022. Resolving the "Muddle in the Middle": the case for *Homo bodoensis* sp. nov. Evol. Anthropol. 31, 20–29.
Schlager, S., 2017. Morpho and Rvcg–Shape analysis in R: R-Packages for geometric morphometrics, shape analysis and surface manipulations. In: Zheng, G., Li, S., Székely, G. (Eds.), Statistical Shape and Deformation Analysis. Academic Press, Cambridge, pp. 217–256.
Schliep, K.P., 2011. phangorn: phylogenetic analysis in R. Bioinformatics 27, 592–593.
Schwartz, J.H., Tattersall, I., 2005. The Human Fossil Record, Craniodental Morphology of Genus *Homo* (Africa and Asia), Vol. 2. John Wiley and Sons, New York.
Schwartz, J.H., Tattersall, I., 1996. Significance of some previously unrecognized apomorphies in the nasal region of *Homo neanderthalensis*. Proc. Natl. Acad. Sci. USA 93, 10852–10854.
Semaw, S., Rogers, M.J., Simpson, S.W., Levin, N.E., Quade, J., Dunbar, N., McIntosh, W.C., Cáceres, I., Stinchcomb, G.E., Holloway, R.L., Brown, F.H., Butler, R.F., Stout, D., Everett, M., 2020. Co-occurrence of Acheulian and Oldowan artifacts with *Homo erectus* cranial fossils from Gona, Afar, Ethiopia. Sci. Adv. 6, eaaw4694.
Shen, G., Gao, X., Gao, B., Granger, D.E., 2009. Age of Zhoukoudian *Homo erectus* determined with $^{26}Al/^{10}Be$ burial dating. Nature 458, 198–200.
Slice, D., 2007. Geometric morphometrics. Ann. Rev. Anthropol. 36, 261–281.
Sokal, R.R., 1958. A statistical method for evaluating systematic relationships. Univ. Kans. Sci. Bull. 38, 1409–1438.
Storm, P., Aziz, F., de Vos, J., Kosasih, D., Baskoro, S., van den Hoek Ostende, L.W., 2005. Late Pleistocene *Homo sapiens* in a tropical rainforest fauna in East Java. J. Hum. Evol. 49, 536–545.
Stringer, C., 2012. The status of *Homo heidelbergensis* (Schoetensack 1908). Evol. Anthropol. 21, 101–107.
Stringer, C., 2002. Modern human origins: progress and prospects. Philos. Trans. R. Soc. B 357, 563–579.
Suwa, G., Asfaw, B., Haile-Selassie, Y., White, T., Katoh, S., WoldeGabriel, G., Hart, W.K., Nakaya, H., Beyene, Y., 2007. Early Pleistocene *Homo erectus* fossils from Konso, southern Ethiopia. Anthropol. Sci. 115, 133–151.
Swisher, C.C., Curtis, G.H., Jacob, T., Getty, A.G., Suprijo, A., Widiasmoro, 1994. Age of the earliest known hominids in Java, Indonesia. Science 263, 1118–1121.
Tattersall, I., 2000. Paleoanthropology: The last half-century. Evol. Anthropol. 9, 2–16.
Toro-Moyano, I., Martínez-Navarro, B., Agustí, J., Souday, C., de Castro, J.M.B., Martinón-Torres, M., Fajardo, B., Duval, M., Falguères, C., Oms, O., 2013. The oldest human fossil in Europe, from Orce (Spain). J. Hum. Evol. 65, 1–9.
Vialet, A., Guipert, G., Alçiçek, M.C., de Lumley, M.-A., 2014. La calotte crânienne de l'*Homo erectus* de Kocabaş (Bassin de Denizli, Turquie). L'Anthropologie 118, 74–107.
Vialet, A., Guipert, G., Cihat Alçiçek, M., 2012. *Homo erectus* found still further west: Reconstruction of the Kocabaş cranium (Denizli, Turkey). C. R. Palevol 11, 89–95.
Vialet, A., Prat, S., Wils, P., Cihat Alçiçek, M., 2018. The Kocabaş hominin (Denizli Basin, Turkey) at the crossroads of Eurasia: New insights from morphometric and cladistic analyses. C. R. Palevol 17, 17–32.
Weber, G.W., 2015. Virtual anthropology. Am. J. Phys. Anthropol. 156, 22–42.
Weber, G.W., Bookstein, F.L., 2011. Virtual Anthropology: A Guide to a New Interdisciplinary Field. Springer, Wien.
Wold, S., Esbensen, K., Geladi, P., 1987. Principal component analysis. Chemometr. Intell. Lab. Syst. 2, 37–52.
Xiao, J., Jin, C., Zhu, Y., 2002. Age of the fossil Dali Man in north-central China deduced from chronostratigraphy of the loess–paleosol sequence. Quat. Sci. Rev. 21, 2191–2198.
Yokoyama, Y., Falguères, C., Sémah, F., Jacob, T., Grün, R., 2008. Gamma-ray spectrometric dating of late *Homo erectus* skulls from Ngandong and Sambungmacan, central Java, Indonesia. J. Hum. Evol. 55, 274–277.